

Parity Violation and Observables for the Hunting Thereof



Zachary R. Hulcher

Supervisor: Dr. Christopher Lester

Department of Physics
University of Cambridge

This thesis is submitted for the degree of
Mphil in Physics

I would like to dedicate this thesis to my loving parents and little brother, to Dr. Krishna Rajagopal, Dr. Daniel Pablos, and to Dr. Joseph Profio, without all of whom I would never have made it this far.

Declaration

I hereby declare that except where specific reference is made to the work of others, the contents of this dissertation are original and have not been submitted in whole or in part for consideration for any other degree or qualification in this, or any other university. This thesis is my own work and contains nothing which is the outcome of work done in collaboration with others, except as specified in the text and Acknowledgements. This thesis contains fewer than 15,000 words not including appendices, bibliography, footnotes, and tables and has fewer than 150 figures.

Zachary R. Hulcher
November 2018

Acknowledgements

I would like to acknowledge and thank Dr. Lester, who was there whenever I needed or asked to talk about the path forward, weekend or weekday. He was a never-ending source of expertise and help. I would also like to acknowledge the ATLAS graduate students, especially Ben Brunt, Chiao-Ying Lin, James Cowley, and Holly Pacey who were my guides through the sometimes nonintuitive world of ATLAS data retrieval, processing, and understanding. I would like to thank my unnamed spaghetti-code latex editor which fails to render the Δ on $\Delta\eta$ on perfectly fine .png files although the .pdf has no problem. You taught me the true depths of spaghetti and encouraged me to code better for it. Thank you to my analysis software, for being marginally less spaghetti than that, but not by much.

Abstract

One of the main points of concern at the Large Hadron Collider (LHC) and future high energy colliders is the subject of beyond the Standard Model physics. Although advances in the neutrino sector with respect to their masses and the hunt for dark matter and dark energy definitely add more to the picture, these and other already-accounted-for experimental signatures cannot account for all of the new physics necessary to rework the Standard Model into a complete model of the universe. Herein we search for signs of excessive parity violation, something already part of the Standard Model, but whose presence in measurements at the LHC in certain regimes either provides constraints on new physics beyond the Standard Model or hallmarks its discovery. We begin with a discussion of the overarching problem, and then move into a discussion of what sorts of observables we may want to use for such an analysis. We analyze possible ways that detector effects could introduce these sorts of signals in possible parity sensitive observables. We analyze the effect that alignment errors can have on the parity sensitivity of the detector, which could be sensitive to certain transformations from a perfect cylinder which also happen to be impossible to see from track reconstruction: weak modes. We also analyze what other sorts of possible detector imperfections could cause such a signal, like detector inefficiencies in unfolding and compare the resulting patterns to measurements in dilepton and jet data from ATLAS.

Table of contents

List of figures	xiii
List of tables	xv
1 Introduction	1
1.1 The Marvel of the ATLAS Detector	2
1.2 Parity Violation for Everyone	4
1.3 The Weak Sector	6
1.4 Beyond the Standard Model Physics	8
2 Special Parity Observables	11
2.1 Two-Particle Observables	12
2.2 Three-Particle Observables	15
3 ATLAS Data Observations	19
3.1 Object Selection	19
3.1.1 Lepton Selection	19
3.1.2 Jet Selection	20
3.1.3 Applicability of Observables	20
3.2 Dilepton, Dijet, and Jet Triad Data	21
3.2.1 Dilepton Observables	22
3.2.2 Dijet Observables	22
3.2.3 Jet Triad Observable	25
3.2.4 Summed Results	27
4 Parity Violation from the Detector?	29
4.1 Effects of Weak Modes on Tracks	29
4.1.1 Effects of Twists in Observables	33
4.1.2 Effects of Other Weak Modes on Tracks	38

4.2	Detector Inefficiencies	41
4.3	Theories and Speculations	42
5	Conclusion	45
	References	47
	Appendix A Twists in the Inner Detector	49
A.1	Charged Relativistic Particles in Magnetic Fields	49
A.2	Effects of Twists on Curved Tracks	50

List of figures

1.1	The important subsystems of the ATLAS detector	3
1.2	The Wu experiment	6
1.3	The Wu experiment	8
1.4	A view of the simplest rendition of the 2 spoons and a fork model	9
2.1	Example of a set of three jets or particles forming a right-handed structure .	17
3.1	Various dilepton τ plots	23
3.2	Various dilepton ζ plots	24
3.3	Dimuon τ plots with η restrictions	24
3.4	Various dijet observable plots	25
3.5	Various dijet τ plots with η restrictions	26
3.6	A plot of the jet triad observable, Λ	26
4.1	The weak modes of the ATLAS inner detector [1]	30
4.2	The effect of a $s = 0.003/\text{m}$ twist on 50 GeV particles with positive η	32
4.3	Effect of twists on ζ in our Monte-Carlo	34
4.4	The effect of twists on ζ plotted as a function of $\Delta\eta$ and $\Delta\phi$	37
4.5	A sample of the possible effects of clamshell deformations on τ from Monte-Carlo	40
4.6	Effects of various example detector inefficiencies on τ	43

List of tables

3.1 Total parity violation statistic, O_{tot} , for our samples 27

Chapter 1

Introduction

Parity violation, or the idea that nature has written into its laws a notion of left and right, and fundamentally, a way to define the notion of left and right in terms of physical processes, is an important and necessary part of the electroweak interactions and thus, the Standard Model of particle physics. However, it was not always so, and parity was once thought an unassailable symmetry of the universe, with Richard Feynman even betting 50 dollars that it was a true symmetry [2]. This type of parity is intricately linked with the spin and angular momentum of the constituent particles and interactions, but herein, we will be looking for more general parity violation in the ATLAS detector, which is, at least at measurement level, independent of this information. Does the ATLAS detector measure events which, more often than not, can be described as left or right-handed?

One of our first discussions involves what it means to be left or right-handed in a general experiment, and we discuss how interesting, if slightly toy, models which could theoretically apply at high energy, could introduce this left or right-handedness to our events. In order to probe this question, we will require a class of observables which are sensitive to our general parity violation, and their general properties will be discussed. We then will look for this parity violation signature as a whole and also in different regions of the ATLAS detector, which could introduce parity violation at the local level. We will perform this analysis with both jet and lepton events for our suite of observables. Then, based on the results of this analysis, we will examine possible ways a false positive in our parity violation observable could be introduced at the local level in the ATLAS detector. Naturally, we begin in the arena in which our data is taken, the ATLAS detector.

1.1 The Marvel of the ATLAS Detector

In this thesis, we will be working with parity-sensitive observables in different angular regions of the ATLAS detector, and so it is important to understand the structure and coordinates of the detector, not only so we can properly work with these observables within a picture of the physical detector, but also so we can later understand what elements of the detector could produce signals in our variables which mimic parity violation. Thus it is necessary to briefly discuss some of the most important aspects of the ATLAS detector.

The ATLAS detector, shown in Figure 1.1a, is a very complicated and very expensive machine for making the precise measurements needed for particle physics. It can be thought of, at the highest level, as a series of concentric cylinders which are, themselves, capped by a series of endcaps, and every time a particle travels through a piece, an energy hit is possibly recorded, or a particle is absorbed. Like any good set of cylinders, we can describe the geometry of the detector in a couple different ways. First, the ATLAS detector lies deep underground on the beamline of the gigantic circular Large Hadron Collider (LHC), and we define coordinates relative to this. The x -axis points horizontally into the center of the ring, transverse to the beamline, while the y -axis points vertically in the same transverse plane. The direction along the beamline, z , is defined such that this coordinate system is right-handed. We also work with a cylindrical coordinate system, parameterized by $\{\eta, \phi, r\}$. r and ϕ are the coordinates of the transverse $x - y$ plane with r the radial component and ϕ starting in standard position. η is the pseudorapidity, defined in terms of the angle starting at the positive z -axis and increasing to the transverse plane, θ , as $\eta = -\ln(\tan(\theta))$. This means that the transverse plane has $\eta = 0$, and the positive z axis sits at $\eta = \infty$.

Because of the massive cost per volume of the detector materials, and because of the importance of getting high precision measurements closest to the collision vertex, the inner detector, whose cross section is shown in Figure 1.1b, records the most accurate measurements of the initial stages of the event. The pixels are the most precise parts of the detector, with each of the 4 cylindrical layers full of $50 \times 400 \mu\text{m}$ pixels, while the SCT (SemiConductor Tracker) is effectively a lower budget, lower resolution pixel system composed of 12 cm silicon strip detectors. The TRT (Transition Radiation Tracker) provides a semi continuous tracking measurement of charged particles as they travel through the series of small tubes and ionize the gas cocktail inside. In practice, particles like muons will not be Lorentz-boosted enough to consistently be tracked, so this detector mostly looks for electrons [5].

Just outside this are the liquid argon ECAL and the liquid argon and tile hadronic calorimeters, which absorb the total energy deposits from charged non-hadrons minus muons, and hadrons respectively. These two systems do much of the work of identifying particles from the resultant distribution of energy deposits [6].

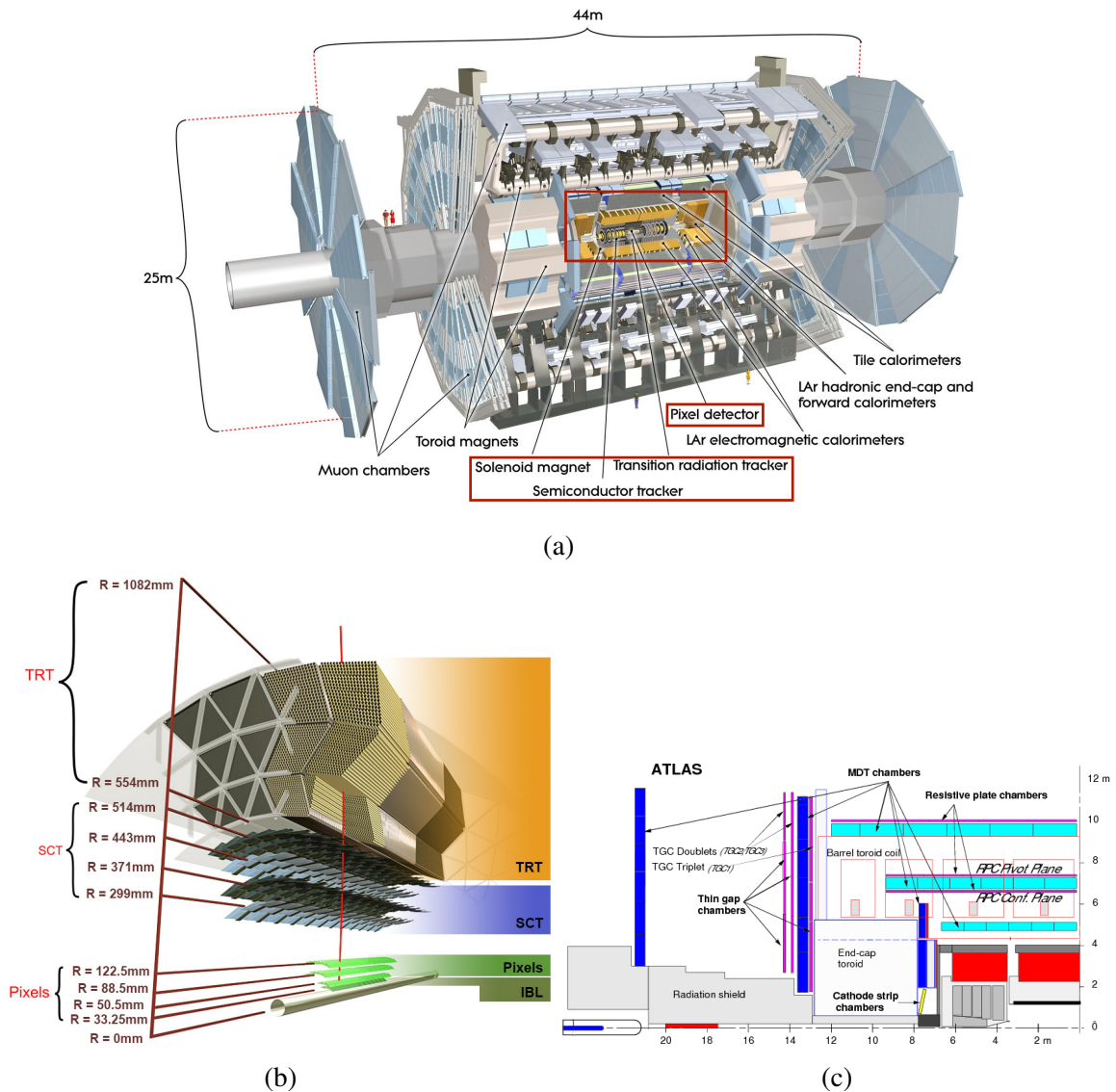


Fig. 1.1 Figure 1.1a is a model of the ATLAS detector [3], one of only a few places in the world where you too can play "The World's Worst Game of Connect-The-Dots"TM. The boxed section, the inner detector, is shown in more detail in Figure 1.1b, and consists of multiple layers of detector which provide very precise measurements of the p_T of electromagnetically interacting particles like electrons, muons, and photons [3]. Figure 1.1c shows an η map of the ATLAS detector, and explicitly shows the boundaries of the systems devoted to capturing more precise information about the muons which are not absorbed by the EM calorimeters closer to the collision center [4]. The RPC and MDT systems form the core of this muon spectrometer system, which enables the measurement of muon total momentum with greater accuracy.

Notably absent is the neutrino, which ATLAS is not designed to detect. But also notably absent are the muons. Muons are special, and get their own systems which make up the outside of the detector. Here, giant toroid magnets produce a magnetic field which is now directed in an angular fashion around the beam line, and this enables an accurate measurement of the muon total energy from the resultant curvature. This curvature is measured by the muon spectrometer system, composed of MDT (Monitored Drift Chamber), RPC (Resistive Plate Chamber), CSC (Cathode Strip Chamber), and TGC (Thin Gap Chamber) layers, which act as additional layers the muons can pass through in this outer magnetic field for the purposes of momentum measurements and triggering. The muon spectrometer system has been upgraded such that below extremely high and low rapidity, $\eta < 2.7$, every muon must hit at least 3 points on this system as it traverses to the freedom of the ATLAS cave wall [7], as shown in the η cross-section of the ATLAS detector in 1.1c.

1.2 Parity Violation for Everyone

Understanding the symmetries of the Standard Model underlies almost all of our understanding of the fundamental interactions of the universe. Symmetries constrain the forms of interactions among particles and ensure that certain properties of theories are conserved at all energy regimes. As the Standard Model is a relativistic quantum theory, the full set of symmetries of special relativity in 3+1 dimensions, the Poincaré group, includes much of the important symmetries of the Standard Model. The Poincaré group is a Lie Group with 10 generators; the ones continuously connected to the identity comprise many of the more recognizable symmetries like rotation and translation isometries as well as boost isometries [8].

Additionally, the $\mathbb{Z}(2)$ transformations which are not continuously connected to the identity, when added to the already mentioned set, comprise the full Poincaré Group. These are transformations like parity flipping, charge conjugation, and time reversal. The Standard Model is known not to be even under charge conjugation, $\psi \rightarrow -i\gamma_2\psi^*$, as left-handed neutrinos, which could interact under the weak force, would turn into left-handed antineutrinos, which have no interactions under the weak force. Parity violation, or non-invariance of physics under flipping the sign of a single spatial coordinate of the system (in odd spatial dimensions this is equivalent to flipping the sign on every spatial coordinate), which takes left-handed particles to right-handed particles, was also famously discovered in the weak force in low energy experiments by Wu. The combination of charge and parity is also known to be violated via a phase in the CKM matrix which comes about because there are 6 left-handed quarks, and by the CPT theorem this means time reversal is violated as well [8].

So why would looking for these already-discovered violations in the LHC be interesting? First, the energy levels of the LHC are enormous, and engineering constraints limit what theoretically should be seen. For example, due to the number of particles in a bunch and the oscillating magnetic fields which cause the acceleration, it is impossible to ascertain the helicity of the incoming protons or lead atoms or the like. On top of that, when the final particles leave an energy signature in a calorimeter or simply leave the detector, they do so in a way which does not record their chirality, helicity, or any similar information about the spin state in the detector. This is reflected by LHC amplitudes being spin-averaged over initial spin states, while final particle spin information is summed over. Thus LHC cross-sections lose information about the spins of particles, so a result like Wu's low energy work, which depended on the initial spin information could not be measured at the energies of the LHC [8].

But this is the type of parity violation which is captured by the Standard Model. Once we have summed over this information, any parity violation is either a feature of the detector, a defect of the detector, or a hallmark of new BSM physics. The ATLAS detector is ideally rotationally invariant about the beam axis, and when colliding proton-proton, the entire LHC is ideally parity invariant, before the magnetic field is turned on. The 2 Tesla magnetic field in the inner detector serves to enable calculation of p_T to a greater precision than could be obtained, if at all, from having to measure p_z . Static magnetic fields do not inherently alter the collision physics, i.e. the initial eta, phi, and energy of the particles emanating from the collision or change the differential cross section for any known particles. Thus, as long as we do not care about physics away from the collision, the magnetic field does no damage to the ideal parity invariance of the system. Thus, parity violation is no feature of the ATLAS detector, and any measurement of parity asymmetry, like high energy electrons tending to come out more pointed towards my old apartment outside of Geneva rather than away from it, would signal something afoot at high energies in the detector.

Extensive searches in new regimes are completely necessary in physics. Madame Wu's hallmark finding of parity violation in the weak sector was motivated by a relatively unnoticed paper from Lee and Yang which simply stated that the strong nuclear force and QED were both parity invariant, but no such study had been made of the weak force. This culminated in Lee and Yang receiving the Nobel prize and Wu earning numerous awards as well as the respect of the entire physics community. With the state of today's physics, where any measurement which departs from Standard Model predictions would ignite furious research, until we verify our assumptions with experiments, no physically possible extension of the Standard Model can be ruled out a-priori [2].

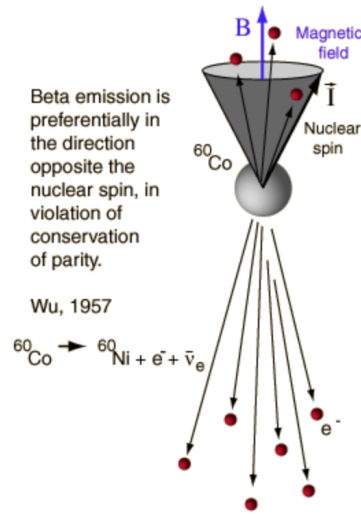


Fig. 1.2 The Wu experiment [9]

1.3 The Weak Sector

For a long time after the discovery of quantum mechanics, and even after QED was formulated and the weak and strong force discovered, the idea that parity was one of the fundamental symmetries of the universe was almost unquestioned. That was until the infamous Theta-Tau puzzle, the problem of the supposed existence of two particles with exactly the same lifetimes, masses, and quantum numbers except for parity. This led Feynman to guess that this could be that one particle had two parity states, and that parity in this particle, now called the kaon, was not conserved. Lee and Yang then searched over the available experimental data, discovering that while QED and the strong force showed no evidence of parity violation, the weak force showed no evidence of parity conservation, but nobody before had searched as they were convinced that it was a law of nature akin to energy conservation. Their landmark paper issued a challenge to test for parity violation in the weak sector, which was taken up by Madame Wu, who looked at the β decay of an ensemble of Cobalt 60 nuclei to Nickel 60, keeping track of the direction of the decay products, as shown in Figure 1.2. If the atoms were just a spin-incoherent radiation source, then the rotational invariance of the ensemble would dictate that there should be no obvious patterns in the distribution assuming QFT was valid. The trick was to place the system in a magnetic field to align the spins and then supercool the nuclei down to where thermal fluctuations would not be an issue [2].

Spin, like orbital angular momentum, is an axial vector. Under parity transformations in 3 spatial dimensions, normal vectors pick up a sign, while axial vectors do not. For orbital angular momentum this is easily understood from the fact that while \vec{r} and \vec{p} are proper

vectors, $\vec{L} = \vec{r} \times \vec{p}$ picks up signs from both of them, which cancel out. For spin, the algebra of SU(2) dictates this same property as it dictates it for orbital angular momentum. The dot product of an axial vector with a proper vector is now not a scalar but a pseudoscalar. Madame Wu used a pseudoscalar formed by the projection of the electron momentum onto the spin axis of the nuclei held in position by the magnetic field. Her team measured the rate of electron production at a particular angle θ measured from the spin axis, which corresponded to the real-world experiment. They then flipped the magnetic field, thereby flipping the spins of the particles, but measured in the same place, which was now $\pi - \theta$ from the spin axis, which corresponded to the mirror world where only the spin direction would have changed. There was a different electron production rate for the “mirrored” angles relative to the spin axis, and thus, parity violation was now an extra ingredient to be incorporated into physics [2].

This had numerous consequences on the development and final implementation of the Standard Model. The original Fermi-4 Theory, a very successful low energy description of the weak interactions, with Lagrangian $\mathcal{L} = G_F (\bar{\psi}_p \gamma_\mu \psi_p) (\bar{\psi}_e \gamma^\mu \psi_\nu)$, coupled the two vector currents in parenthesis, in analogy to QED, which coupled a vector current $J_V^\mu = \bar{\psi}_1 \gamma^\mu \psi_2$ to the vector potential A_μ . It was extremely successful in describing β decay and unifying it with a whole host of other interactions and processes characterized by electrons, protons, muons, neutrinos, and their antimatter partners. However, Madame Wu’s and subsequent experiments indicated that the weak force was maximally parity violating, as it involves only left-handed particles and right-handed antiparticles. To incorporate this parity violation required the addition of axial currents $J_A^\mu = \bar{\psi}_1 \gamma^\mu \gamma^5 \psi_2$. Specifically, experiments dictated that interactions should be couplings of $J_V^\mu - J_A^\mu$ terms, or terms of the form $\bar{\psi}_1 \gamma^\mu (1 - \gamma^5) \psi_2 = 2\bar{\psi}_1 \gamma^\mu P_L \psi_2$, where P_L projects to their left-handed variety. Because $\{\gamma_5, \gamma^\mu\} = 0$, this implies $\gamma^\mu P_L = P_R \gamma^\mu$, which projects the antiparticle onto its right-handed component, but this is the antiparticle of the left-handed particle. Therefore all of the currents in the weak interaction take the form $\bar{\psi}_{1L} \gamma^\mu \psi_{2L}$ [10].

This product of currents that Fermi postulated and later improved upon is an effective theory which results from taking the low energy limit of the full weak interaction [8]. In the full theory, the massive W^\pm and Z bosons mediate the weak force analogously to QED. These bosons couple to currents like $\bar{\nu}_L \gamma^\mu e_L$ producing diagrams like the muon-electron interaction shown in Figure 1.3.

The left-handed nature of this force is responsible for all of the parity violation thus far seen. For example, in the process $pp \rightarrow Z/\gamma^* \rightarrow \mu^+ \mu^-$, where a quark-antiquark pair produces a dimuon pair mediated by a Z boson, there is an asymmetry between positive and negative values of the cosine of the angle between the antimuon and the antiquark in the rest

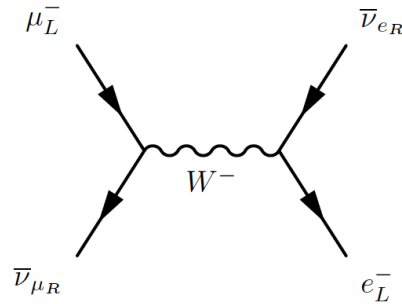


Fig. 1.3 Flavour changing mediated by a W^- boson

frame of the resulting muon pair [11]. This type of parity violation, known as the z forward backwards asymmetry, can be easily seen at CERN, and the experimental data matches up well with Monte-Carlo [11]. Nothing needed to be recorded about the handedness of any particle, (although we know the particles are left-handed-from theory) but the failure of parity resulted just the same. In this case, however, although we can still get this signature in pp collisions at ATLAS, which at first glance do not pick a direction in z , the direction along the beam line is picked statistically by the direction of the longitudinal boost of the resulting leptons, as the participating quark, which is more massive than the participating antiquark, should cause the resulting leptons, more often than not, to be boosted in that direction [11]. This means the collision is $q\bar{q}$, and a direction is picked by the net current vector.

However, could parity violation come from systems where the spin information is explicitly unknown, and no direction can be picked a-priori? Even more interesting, what kinds of parity violation could result from completely symmetric collisions? In this analysis, we will be looking for something a little more exotic, signs of a signal of beyond the Standard Model physics.

1.4 Beyond the Standard Model Physics

Just like the situation before the Wu experiment, measurements of parity violation, this time in the high energy regime, are currently lacking. We highlight some, admittedly toy, ways such a violation could happen while being arguably consistent with other such measurements. At high energy, through some mechanism we will not look into, identifiable components of final state particles could arrange themselves into a triad which is approximately right-handed or left-handed [12]. The identifiable components could be suitably picked jets or leptons in order of increasing p_T or some other variable. Different leading types of leptons or

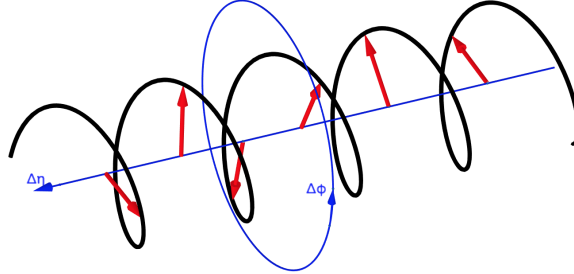


Fig. 1.4 A view of the simplest rendition of the 2 spoons and a fork model, where $\Delta\phi = K\Delta\eta$. This forces particles or jets with a particular difference in η to have a corresponding difference in ϕ and forces results in this geometrical helix as shown.

differently tagged jets could also make up the 3 components necessary for this. We will define an observable for testing this in the next chapter.

A more esoteric example is the possibility of a mechanism at high energy that, while preserving energy-momentum, changes the probability distribution over η and ϕ in the following way: the particles find themselves in three separate groups in the theory, two are the "spoons," while the third is the "fork." These groups organize themselves along the collision such that the spoon groups' total momentum directions have a difference in ϕ which is proportional to their difference in η [13]. We require the fork in order to conserve momentum in the general case. What this does is constrain the spoons to lie on something resembling a geometric coil or screw-thread as in Figure 1.4. Notice that this model does not introduce any angular or beam line anisotropies, but only correlates the transverse and longitudinal degrees of freedom. We could also change the details such that the spoons and forks are distributions with their mean satisfying the above property relating $\Delta\eta$ and $\Delta\phi$, and we could equally well enforce the proportionality to be between $\Delta\eta$ and, for instance an increasing function of $\Delta\phi$, which would deform the screw and add some thickness. This is far from the only way to introduce parity violation in events. We could simply change the form of the explicit parity violation to be, for example, of the form $p_{x1}p_{y2} - p_{y1}p_{x2} = K(p_{z1} - p_{z2})$, which sets the sine of $\Delta\phi$ proportional to something which is almost Δz , but many factors of different P_T are mixed in [14]. In general, there are an infinite family of different possible parity violation constraints, and consequently an equally large family of different observables to go along with them with different sensitivities to other effects.

Chapter 2

Special Parity Observables

In general, a parity sensitive observable is any function of any observable quantity which is odd under flipping one of the axis directions. For our purposes, we will have to make some choices to limit this infinitely large space of observables we could use to measure this effect based on nice properties we may want our observables to have. For our dilepton and dijet observables, we will want them to be even under interchange of the leptons or jets, and for the trijet observable, we will need it to be odd under interchange so that the observables can measure parity violation instead of anisotropy. Once we derive these observables, we will discuss why these properties are important.

We would also like observables which are relatively insensitive to other possible sources for a parity signature. This is a much more amorphous requirement, as the number of constraints is as large as the space of possible ways to "trick" any observable. For starters, parity violation can occur without breaking the symmetries of the restricted Lorentz group, or rotation and boost symmetries; also the ATLAS detector is constructed in such a way that ideally, when colliding pp or PbPb, it is rotationally invariant around the transverse ϕ plane, and other than the magnetic field, which should not affect the dynamics of the initial collision, the detector does not pick out a preferred direction along the beam line z -axis a-priori. Therefore, since any observable parity violation effect coming from slight rotational variances or slight z direction preferences would not result from true parity violation, and any direction possibly picked out by the $q\bar{q}$ collision would be split evenly over many events, observables which are less sensitive to these sources of parity violation are preferred. We also need observables which are comparable with one another, and therefore, we need scalar quantities, like ϕ or $|p_a|$. We cannot form truly parity sensitive observables from only the information from one particle, as it will only highlight anisotropy in some direction. Thus we must at minimum look at information from two particles.

2.1 Two-Particle Observables

For two particle observables, we will have to choose observables which are not completely rotationally symmetric under an arbitrary 3D rotation, or those which choose a particular undirected axis in space. Let us look at a case which will correspond to the observables we will use. Let us look at the case when $p_{x1}p_{y2} - p_{y1}p_{x2} = K(p_{z1} - p_{z2})$ for a particular event, where K is a constant with units of momentum. This equation picks out the z -axis from the other two. Can the relations which pick out the other two axes be true at the same time? Let us define for ease of use, the following:

$$A = p_{x1}p_{y1}p_{z1} + p_{x2}p_{y2}p_{z2}$$

$$B = p_{x1}p_{y1}p_{z2} + p_{x2}p_{y2}p_{z1}$$

$$C = p_{x1}p_{y2}p_{z1} + p_{x2}p_{y1}p_{z2}$$

$$D = p_{x1}p_{y2}p_{z2} + p_{x2}p_{y1}p_{z1}$$

Rotations can take, for example, $p_x \rightarrow p_y$, $p_y \rightarrow p_z$, and $p_z \rightarrow p_x$, and under this, $A \rightarrow A$, $B \rightarrow D$, $D \rightarrow C$, and $C \rightarrow B$. This means that under this rotation, $C - D \rightarrow B - C$ and $B - C \rightarrow D - B$. We see that if we add together $(C - D) + (B - C) + (D - B)$, this is identically 0. However, $C - D$, assuming the hypothesized parity violation, is also $K(\Delta p_z)^2$. Performing the rotations on $B - C$ and $D - B$, we see that these terms are $K(\Delta p_x)^2$ and $K(\Delta p_y)^2$, respectively, if we assume the relation above is true for all choices of axis at the same time. $K((\Delta p_x)^2 + (\Delta p_y)^2 + (\Delta p_z)^2) \neq 0$ in general, so we cannot have all three of these parity violation equations being true at once. The event must pick an undirected axis in space, which conveniently is supplied by the beam axis, while leaving a rotational symmetry around ϕ . The same result applies if we try to have $\Delta\eta = K\Delta\phi$; if we try to have this constraint be true and also rotationally invariant, we add two more independent constraints on our variables $\Delta\eta$ and $\Delta\phi$; in other words, the system is too constrained. In general, this comes because the collision and the corresponding particles define a plane and can possibly define an orientation on that plane. In our case, this plane is the transverse plane, and if the particles' momenta are mirrored about any axis in the plane, the orientation can be unambiguously flipped accordingly. However, if we allow the particles to rotate through the z axis, then that parity flip followed by a rotation through z would return the system to the same picture, but the orientation we defined on the plane would be flipped, making a definite orientation meaningless. Thus, any true parity violation which this two-variable observable finds should

be a result of interference effects which single out this axis. It is very important that this axis has no preferred direction. Crucially, this means that parity observables should still have to be odd under a flip of any z momentum directions in the observable.

Even with these observations, this leaves wide open the space of two-particle observables which could be tailored to searching for parity violation at the LHC. Herein, we will focus on two observables which are motivated also by measurable quantities. The LHC measures the p_T as well as the angles ϕ and η for each track. We can convert this into the components of momentum along each axis in any coordinate system, p_x , p_y , and p_z . We have already noted that we must have information from two particles in our observable, as no non-anisotropy parity information can be encoded in the dynamics of one particle if the spin information is not recorded. Differences in any of the above observables between two particles, like $p_{z1} - p_{z2}$ are similarly problematic, as they also only record parity violation indistinguishable from anisotropy. The product $\phi\eta$ for a particular event, which is effectively the product of the differences between that particle's cylindrical coordinates and one with $\phi = 0$ and $\eta = 0$, is a better choice, but if this were to find anything, it would not just choose the z axis, but also the $\phi = 0$ direction where the sign changes, so it would highlight anisotropy. However, we can choose a similar construction, where we take the product of the difference in the angles between two events, $\Delta\phi\Delta\eta$, which would be maximally sensitive to a parity violating effect favoring something like $\Delta\phi = K\Delta\eta$, but would not a-priori pick out any signed direction in space.

Having ruled out linear combinations of momentum due to their undesirable properties, if we want to construct a parity violating observable out of momentum projections, we are forced to use at least linear combinations of momenta products. We also will be forced to make these products of three different momentum directions, as the observable, in order to be a valid parity observable, should change sign under any flip of an axis. We have p_x , p_y , or p_z of both particles to work with. Terms which are not at least linear in each momentum direction, like $P_{x1}^2 P_{x2}$ or $p_{z1} p_{z2} p_{x1}$, will not contribute to good parity observables as explained previously as the terms must change sign under each direction separately flipping orientations. We again want to work with terms which are invariant under particle swapping. All possible terms, which we are free to take linear combinations of, are exactly the observables A through D above.

If we then enforce the rotational symmetry around ϕ , or equivalently $x \rightarrow y$ and $y \rightarrow -x$, and its opposite transformation, then we are left with only $C - D = (p_{x1} p_{y2} - p_{x2} p_{y1})(p_{z1} - p_{z2})$. $C - D$ would take a constant sign when $\sin(\Delta\phi) = K(p_{T1} \sinh \eta_1 - p_{T2} \sinh \eta_2)$, which is very close to a rescaling of $\Delta\phi = K\Delta\eta$. This looks like it is indeed hunting for proper parity violation of some kind. Thus, independent of a particular form of parity violation,

the simplest possible parity sensitive observable constructed from momentum projections is $C - D$.

To see this another way, if we construct an observable, the mean value of the observable assuming whatever parity violation is a good measure of the parity violation signature. For example, let us again use the example parity violation of $p_{x1}p_{y2} - p_{y1}p_{x2} = K(p_{z1} - p_{z2})$, and let the constant in front of term A be O_A , etc. The mean of an arbitrary observable consisting of these 4 terms under the given parity violation is $\frac{O_C - O_D}{4K} \langle p_T^2 \rangle^2$. The important part is that we don't get any signal unless either O_C or O_D is nonzero, and any other terms contribute nothing. Even worse, any other terms contribute to the standard deviation of the mean, which obstructs the measurement of the mean.

There is one more interesting thing of note. The choice of whether to use a variable which is even under particle exchange vs one which was odd may have seemed an arbitrary, if possibly well motivated one. However, one can see from the appropriately modified terms A-D with minus instead of plus signs that it may be necessary for a proper observable. We can still remove the new terms $A^{(-)}$ and $B^{(-)}$ because they cannot be combined to be rotationally invariant in the transverse plane. The only valid rotationally invariant term is $C^{(-)} + B^{(-)} = p_{T1}p_{T2} \sin(\Delta\theta)(p_{z1} + p_{z2})$. This observable looks for when the sine of the difference in ϕ is correlated with whether the particles are pointing more in positive or negative η , a manifestation of anisotropy. Taking a step back, because of the rotational symmetry in the transverse plane, and the necessity of including $\Delta\phi$ information, any valid parity sensitive observable must have its angular information be composed entirely of functions of $\cos(\Delta\phi)$ and/or $\sin(\Delta\phi)$. Because of our assumption that nothing in the collision picks a direction, and because of the complex processes which can affect the production and identification of either back-to-back or more collinear jets or leptons, we have argued that there should be no reason to expect interesting parity effects to come from whether jets or leptons face a similar direction or are more back-to-back. Also, any true parity sensitive observable should change sign upon interchanging the x and y directions, or equivalently, changing the sign on the angle $\Delta\phi$. These reasons mean that every term in a Fourier expansion of the observable is a $\sin^{2n+1}(K\Delta\phi)$ term, or in other words, there are an odd number of sines in each term. But now, on this arbitrary observable, when we change particles, picking up a minus sign, this has to come from the sines in each term and cannot come from any η dependence. This means that any two-particle observable which is even under particle exchange has to be even under $\eta_1 \rightarrow \eta_2$ and vice-versa while holding the ϕ 's constant. Thus, this observable cannot depend on η differences, but only absolute η values, meaning it tests anisotropy.

In summary, for our two-particle observables, we will look at two different observables inspired by the above arguments in our analysis. For the first one, we calculate the η and ϕ differences between the reconstructed leptons or jets and keep the sign of the product, or

$$\tau = -\text{sgn}(\Delta\eta\Delta\phi), \quad (2.1)$$

which looks for $\Delta\phi = K\Delta\eta$, which we shall, from now on, refer to as τ parity violation. For the second, we reconstruct the momenta of the particles or jets in Cartesian coordinates and define

$$\zeta = (p_{x1}p_{y2} - p_{y1}p_{x2})\text{sgn}(p_{z1} - p_{z2}) \quad (2.2)$$

which looks specifically for $p_{x1}p_{y2} - p_{y1}p_{x2} = K(p_{z1} - p_{z2})$, which we shall, from now on, refer to as ζ parity violation. The minus sign in τ is for rough agreement between the observables.

For both observables, we can plot them in multiple different ways. Our principle way, which we will mostly follow throughout this thesis is the method of Dr. Gillam and will plot the number of positive hits of the observable in a bin minus the number of negative hits binned over the η and ϕ for one of the particles in the pair for the event, or $N_p(\phi, \eta) - N_n(\phi, \eta)$ [14]. The expectation value, assuming an ideal detector and no parity violation, is zero across this plot, so we can construct an appropriate normalization. The expected error on this binning is the square root of the number of events in the bin, $\sqrt{N(\phi, \eta)} = \sqrt{N_p(\phi, \eta) + N_n(\phi, \eta)}$, resulting in a plot of

$$O_1(\phi, \eta) = \frac{N_p(\phi, \eta) - N_n(\phi, \eta)}{\sqrt{N_p(\phi, \eta) + N_n(\phi, \eta)}} \quad (2.3)$$

Other plots of our observables will be defined later in the relevant context.

2.2 Three-Particle Observables

This line of thought also works for three-particle observables. Now we have $\{p_{x1}, p_{y1}, p_{z1}\}$, $\{p_{x2}, p_{y2}, p_{z2}\}$, and $\{p_{x3}, p_{y3}, p_{z3}\}$ to work with. We are still in three dimensions, but now we are not limited by the choice of the z -axis, as three identifiable particles or jets define a left-handed or right-handed system and a parity which no rotation can change. This means we can make observables which are fully rotationally invariant in that they do not pick any direction out. For this freedom, however, we have to give up the symmetry we were allowed for particle exchange. The observable is still even, however, under cyclical rotations of the particles. For the same reasons as before, in order for an observable to truly measure parity,

we want terms which change sign if any coordinate axis changes, so we begin with linear combinations of products of three momentum values.

Now, the total number of terms before any constraints is 165. Twenty-seven of these terms depend on each momentum direction, shrinking the total set dramatically. Three of these 27 are $p_{in}p_{jn}p_{kn}$, and 18 of the 27 are $p_{in}p_{jn}p_{km}$ where n and m are particle numbers and i, j , and k are the momentum directions; these terms vanish because they are even under exchanging the i and j directions. This leaves the remaining 6 terms, which combine under the given symmetries and antisymmetries to an observable we will call Λ :

$$\Lambda = p_{x1}p_{y2}p_{z3} + p_{y1}p_{z2}p_{x3} + p_{z1}p_{x2}p_{y3} - p_{x1}p_{z2}p_{y3} - p_{y1}p_{x2}p_{z3} - p_{z1}p_{y2}p_{x3} \quad (2.4)$$

or equivalently,

$$\Lambda = P_{T1}P_{T2}P_{T3}[\cos(\theta_1) \sin(\theta_2) \sin(\theta_3) \sin(\phi_3 - \phi_2) + \cos(\theta_2) \sin(\theta_3) \sin(\theta_1) \sin(\phi_1 - \phi_3) + \cos(\theta_3) \sin(\theta_1) \sin(\theta_2) \sin(\phi_2 - \phi_1)]. \quad (2.5)$$

This is exactly the signed volume of the parallelepiped defined by the three different momentum vectors. Because this observable is explicitly rotationally invariant, if we have three particles or jets, this observable should give the same result no matter which orientation the three-particle structure faces. Let us define a right-handed coordinate system and check that our observable can measure parity. The three-particle configuration can be rotated to the following position: particle 1 can be placed on the x -axis such that θ_1 coming down from the z -axis is $\pi/2$ while ϕ_1 defined coming from the x axis is 0; we can also use our remaining freedom to put particle 2 in the $x - y$ plane such that $\theta_2 = \pi/2$. Thus, our unrestricted coordinates are ϕ_2 , θ_3 , and ϕ_3 . An example set of particles is shown in Figure 2.1. The overall parity of any such system does not depend on ϕ_3 , but it does depend on the other two angles. Putting in these constraints to equation 2.5, we get that the parity of the system is $\cos(\theta_3) \sin(\phi_2)$. This exactly picks out the parity of the system, as we can see from Figure 2.1. With p_1 fixed on the x axis, the system will be right-handed if either $\theta_3 < \pi/2$ and $0 < \phi_2 < \pi$ or $\theta_3 > \pi/2$ and $\pi < \phi_2 < 2\pi$ and left-handed for any other values of the angles except the boundaries which make the handedness undefined, as the configuration would then be contained in a 2D subspace.

The argument for any observable, Λ' , having to be even under the cyclic rotation of 3 particles is easy to justify, as $\Lambda' = (-1)^{3p} \Lambda'$ under the three exchanges where p is even if there is symmetry and odd if antisymmetry. But again, one could make the argument as to

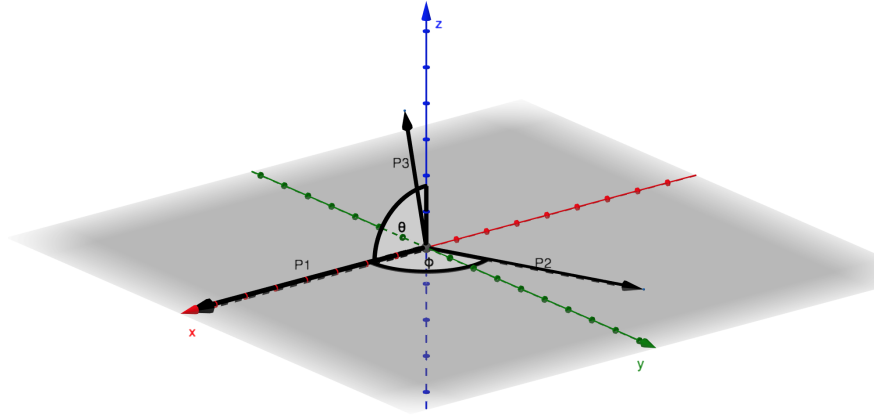


Fig. 2.1 Example of a set of three jets or particles forming a right-handed structure

why we chose that the observable had to be odd under two-particle exchange; after all, the previous sets of observables were required to be even under the same exchange. If we go back to our 165 terms in looking for a valid observable in linear combinations of product triplets of momentum projections, but this time we assume the particles are even under particle exchange, the argument follows in the same way all the way down to just before the remaining 6 terms. However, one can see that the linear combination for Λ' given these 6 terms is dictated solely from the requirements of being even under the cyclic rotation and odd under exchanging any two directions in space. If we add in symmetry under particle exchange, we see that the observable cannot support it, and no observable can be made as a linear combination of product triplets. For general observables, they should assign one parity to particle 1 on the x axis, particle 2 on the y axis, and particle 3 on the z and a different one for the same axes but particles 2 and 3 switched. If the observable was indeed even under particle exchange, it could not separate these two different handed triads, and therefore would be useless to us.

In summary, these are the simplest possible observables using just p_T , ϕ , and η or p_x , p_y , and p_z , but there are still other things we can add in which can affect these observables. For example, we can add in anything which can be measured for a particular particle, including, but not limited to, the charge of the particle, the total particle travel time, etc. We will come back to this near the end of our discussion of twists. We can also extend our limitations by adding arbitrary terms with higher powers of these momenta, like $p_{x1}p_{y2}p_{z3}^3$, as long as we add in other terms such that the relevant symmetries and antisymmetries under particle exchange, axis exchange, and axis flipping are still valid. However, this process quickly makes the number of terms in the observable extremely large.

We cannot use these types of observables to probe parity violation in any higher dimensions, i.e. $\{x, y, z, a\} \rightarrow \{-x, y, z, a\}$, as we only have access to three dimensions of that higher parity violation. Any observable we would be able to construct would have to be odd upon flipping the direction of the 4th or higher dimension, but since we do not have access to it, we trivially cannot construct an observable with this property using this method. We could just rotate any parity flip in one of the observable dimensions out through a rotation in the plane containing that direction and one of the hidden ones. We have also already commented that 1-dimensional parity violation, or anisotropy, is beyond our scope, and two-dimensional parity violation cannot be incorporated into our 3D space. We also have constructed observables for general parity violation with full and partial rotational symmetry in 3D. While there is the possibility of parity violation with no rotational symmetries occurring, what would choose the necessary three directions to break the ambient spatial rotational symmetry is not immediately obvious to me. Other than this possibility, the listed observables should be sensitive to any possible parity violation not associated with known initial spin degrees of freedom.

Chapter 3

ATLAS Data Observations

3.1 Object Selection

Herein we describe the datasets upon which this analysis is based. Both our lepton and jets sets pass through a series of stages and checks, namely pre-selection, overlap removal, and event cleaning/final object selection, and each element of each event is processed differently.

3.1.1 Lepton Selection

In this analysis, 2015 and 2016 dilepton events, taken from skims which had been created by a previous student for his thesis, were used [15]. Over this time period, the ATLAS experiment recorded a total integrated luminosity of 39.5 fb^{-1} . For lepton tracks to be preselected, they must have satisfied a number of requirements. All leptons must have had a calibrated p_T of 10 GeV. In order to have high quality electrons, they must have had $|\eta| < 2.47$ and not have passed anywhere near one of the dead regions of the LA calorimeter. The muons, on the other hand, could have had $\eta < 2.7$. Our leptons sample has ee , $\mu\mu$, and $e\mu$ events, and each event had to pass its own initial isolation requirements, `LooseAndBLayerLLH` for the electrons and `Medium` for the muons [16][17]. The ee , $\mu\mu$, and $e\mu$ from 2015 and 2016 also must have passed dilepton triggers with particular p_T requirements. The $e\mu$ events must have had an electron of at least 17 GeV and a muon of at least 14 GeV. The ee events from 2015 had two electrons of at least 12 GeV while those from 2016 had two of at least 17 GeV. The $\mu\mu$ events from 2015 had two muons of at least 10 GeV while those from 2016 had two of at least 14 GeV.

The next important step is the overlap removal, which generally functions to remove tracks which are on top of other tracks. For example, if a muon and electron shared the same track, then the electron was removed from the event listing, and if a lepton overlapped with

a non-pileup jet, such that the total jet radius was less than 0.4, the lepton was deleted, as it was sitting in the jet. Final selection involved getting rid of tracks which were identified as not coming from the primary vertex. The events were also cleaned by removing any track whose transverse impact parameter was either more than 0.5 mm or too many standard deviations away from the primary vertex, including cosmic muons. We finally enforced that all remaining tracks must have $p_T > 25$ GeV. The resulting leptons were ordered by p_T and formed our lepton data.

3.1.2 Jet Selection

Our jets come from 2017, a year with a total integrated received luminosity of 46.9 fb^{-1} . For our jets, a similar process to leptons occurred, with some subtleties and differences. One of the most important processes was that of the jet vertex tagger (JVT) [18] requirement, which limited valid jets to ones with lower contribution from pileup jets. Also, since jets are collimated collections of particles, we have to have an algorithmic approach to clustering them, which is supplied by the anti- k_r algorithm, and we work with a jet radius of $\Delta R = 0.4$ [19]. Jet events must have all passed a 400 GeV single jet low level trigger. Every jet considered must also have a $p_T > 20$ GeV and $\eta > 2.4$, but the JVT was needed to get rid of jets which were not identified as coming from the primary vertex and had $p_T < 2.4$ and $p_T < 50$ GeV, the intuition being that these tracks were too curvy to be reliably tracked back to a primary vertex without it. Our leading jet must have had a p_{T1} of at least 450 GeV in order to satisfy the single jet trigger requirement and the subleading jet must have had a p_{T2} which satisfied $\frac{p_{T1} - p_{T2}}{p_{T1} + p_{T2}} < 0.3$, or in other words, $p_{T2} > 242$ GeV, such that our dijet events had comparable p_T for each jet. These requirements also limited our set to dijet events of high enough p_T to look for effects not seen at lower energies.

3.1.3 Applicability of Observables

We now ask, would these observables theoretically be able to find the parity violation they are designed to look for in our data? Any parity violation would show up in O_1 as a non-zero mean over the whole plot, with a mean of 0 corresponding to no observable global parity violation. We can construct the standard deviation to mean ratio for ζ and τ themselves, irrespective of a choice of plotting, which is just the inverse of the normal statistic for sample mean testing, $\frac{\mu - 0}{\sigma/\sqrt{N}}$, without the \sqrt{N} factor. If this is not too large ("not too large" defined relative to the square root of the number of available dijet, dilepton, or similar events), then this means that some reasonable amount of data can differentiate a distribution with positive

or negative mean from null and successfully identify the signature. For our observable τ assuming τ parity violation, we get that

$$\frac{\sigma_\tau}{\mu_\tau} = \frac{1}{\sqrt{2}} \sqrt{1 + \frac{\langle \eta^4 \rangle}{\langle \eta^2 \rangle^2}} = \frac{1}{\sqrt{2}} \sqrt{1 + \frac{\langle \phi^4 \rangle}{\langle \phi^2 \rangle^2}}. \quad (3.1)$$

For ζ (where I remove the signum function for mathematical expedience) assuming ζ parity violation, we get that

$$\frac{\sigma_\zeta}{\mu_\zeta} = \frac{1}{\sqrt{2}} \sqrt{1 + \frac{9 \langle p_T^4 \rangle^2}{4 \langle p_T^2 \rangle^4}} \quad (3.2)$$

Thus, it depends on the properties of the spectra of p_T which we measure as to what the overall feasibility of this method is. Because $\frac{\langle p_T^4 \rangle^2}{\langle p_T^2 \rangle^4} > 1$, which can be derived by considering the definition of σ_{η^2} , this observable is at least $\sqrt{1.625} \approx 1.27$. In particular, it depends on how falling the p_T spectrum is in the region in which we measure. If we measure in a region where the spectrum is steeply falling or rising, the fraction inside the square root is approximately 1, and so the standard deviation around the mean is approximately on the order of the mean, and we can more than likely get a clean signal if it exists with a low number of events. However, if the spectrum is relatively flat, then the fraction is almost arbitrarily large, and we have no hope of getting a clean signal in either without making use of very high statistics. Note that this is assuming exactly the type of parity violation that the variable will look for and always be positive for. For general parity violation, these results are a best-case scenario, so ζ can and will overtake τ for many possible parameterizations of parity violation.

Using the 2015-2016 dilepton data, we calculate $\frac{\langle \eta^4 \rangle}{\langle \eta^2 \rangle^2} = 2.80$ and $\frac{\langle p_T^4 \rangle^2}{\langle p_T^2 \rangle^4} = 978.18$. These results mean that $\frac{\sigma_\tau}{\mu_\tau} = 1.38$, while $\frac{\sigma_\zeta}{\mu_\zeta} = 46.92$. For this particular dataset, τ is almost certainly preferred, but with higher cuts on p_T , the balance could shift. However, when we look at our 2017 dijet data, the positions are much more equal, as $\frac{\langle \eta^4 \rangle}{\langle \eta^2 \rangle^2} = 2.89$ and $\frac{\langle p_T^4 \rangle^2}{\langle p_T^2 \rangle^4} = 1.89$, so $\frac{\sigma_\tau}{\mu_\tau} = 1.39$ and $\frac{\sigma_\zeta}{\mu_\zeta} = 1.64$. In general $\frac{\langle p_T^4 \rangle^2}{\langle p_T^2 \rangle^4}$ is a scalable parameter, and we can find other appropriate datasets and cuts to make it a reasonable number such that we can search for these parity effects.

3.2 Dilepton, Dijet, and Jet Triad Data

We will now plot a range of these observables in Figures 3.1 through 3.6. The leptons data are from the 2015-2016 dileptons set referenced earlier, while the jets data are from the 2017

jet dataset also referenced earlier. In each two-particle observable, we take the leading two leptons or jets as input to our observables, while for Λ , we take the leading three jets in order of decreasing p_T . We notice that the plots seem to have some η asymmetry, so we also plot projections of these plots onto ϕ where the components binned in positive η keep the same sign while those in negative η get an extra minus sign on their contribution. The result is then plotted in a way reminiscent of O_1 , or in other words,

$$O_2(\phi) = \sum_{\eta} \frac{(N_p(\phi, \eta) - N_n(\phi, \eta))\theta(\eta > 0) - (N_p(\phi, \eta) - N_n(\phi, \eta))\theta(\eta < 0)}{\sqrt{N_p(\phi) + N_n(\phi)}}. \quad (3.3)$$

3.2.1 Dilepton Observables

We can see there is obvious substructure while plotting τ over all dilepton pairs in Figure 3.1a. Where could this structure be coming from? The sample we have has too low frequency of particles with the same charge or even $e^- \mu^-$, and its opposite to make any statement about whether the relative charges of the particles contribute, as it is dominated by $q\bar{q} \rightarrow Z \rightarrow e^+ e^- / \mu^+ \mu^-$. What we can see from the plots of ζ and τ over $e^+ e^-$ in Figures 3.1 and 3.2 is a random plot with very little in the way of visible structure. The electrons are noise over the now much more pronounced structure of the τ and ζ plots taken over $\mu^+ \mu^-$. There appears to be very interesting visible banded structure which is asymmetric in η . There also seems to be two sets of this η -antisymmetric banded structure, one from approximately $|\eta| > 0.8$ and the other $|\eta| < 0.8$. The exact nature of this structure we have to theorize about, but we can see it more clearly in the figures on the right. There appear to be significant peaks at ϕ values of approximately -2, -1, 1, and 2 radians. We split this up even more in Figure 3.3, to events which are either in the same rapidity half or not, and surprisingly, we see effects in both. Something fishy is going on. In the next chapter, we will explore ideas for how this could come about. Notice that the observables ζ and τ come up with very similar plots.

3.2.2 Dijet Observables

In Figures 3.4a and 3.4c, we see our observables τ and ζ plotted again, but this time for dijet events. There is very visible structure at ϕ values just below 3 and just below 1. The more pronounced structure around 3 is antisymmetric about $\eta = 0$. These are more than likely related, as dijet events have a strong tendency to be back-to-back in ϕ . The exact nature of this structure again, I can only speculate about. Again, we can see that the plots for ζ and τ are very similar, as are their η -antisymmetric plots binned in ϕ but this time the peaks for

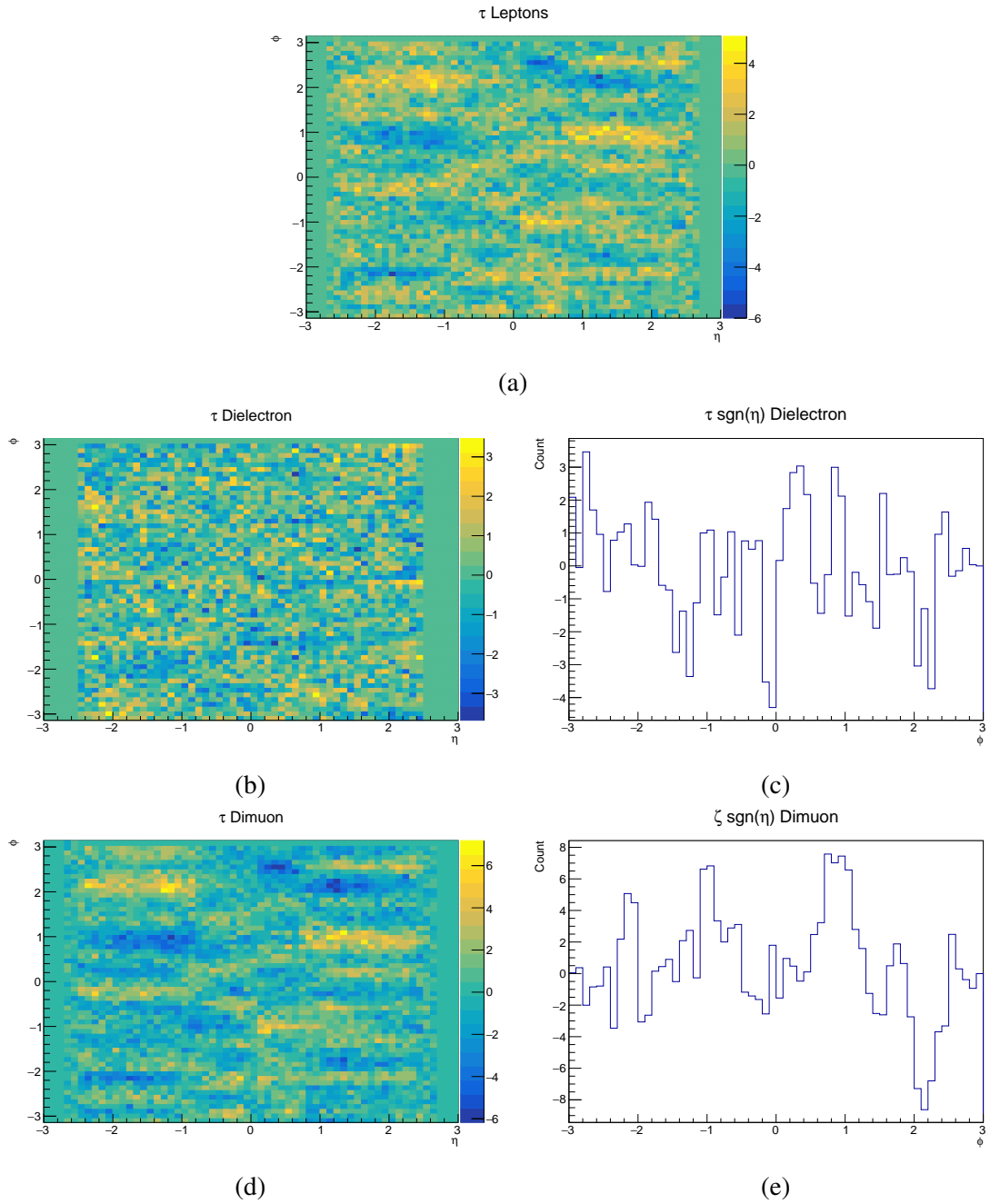


Fig. 3.1 Here we have dilepton τ plots. 3.1a is τ over all leptons. 3.1b is τ over electrons and positrons, while 3.1c is its accompanying ϕ -projection in the η -antisymmetric way described earlier. 3.1d is τ for muons and antimuons, and 3.1e is its ϕ -projection.

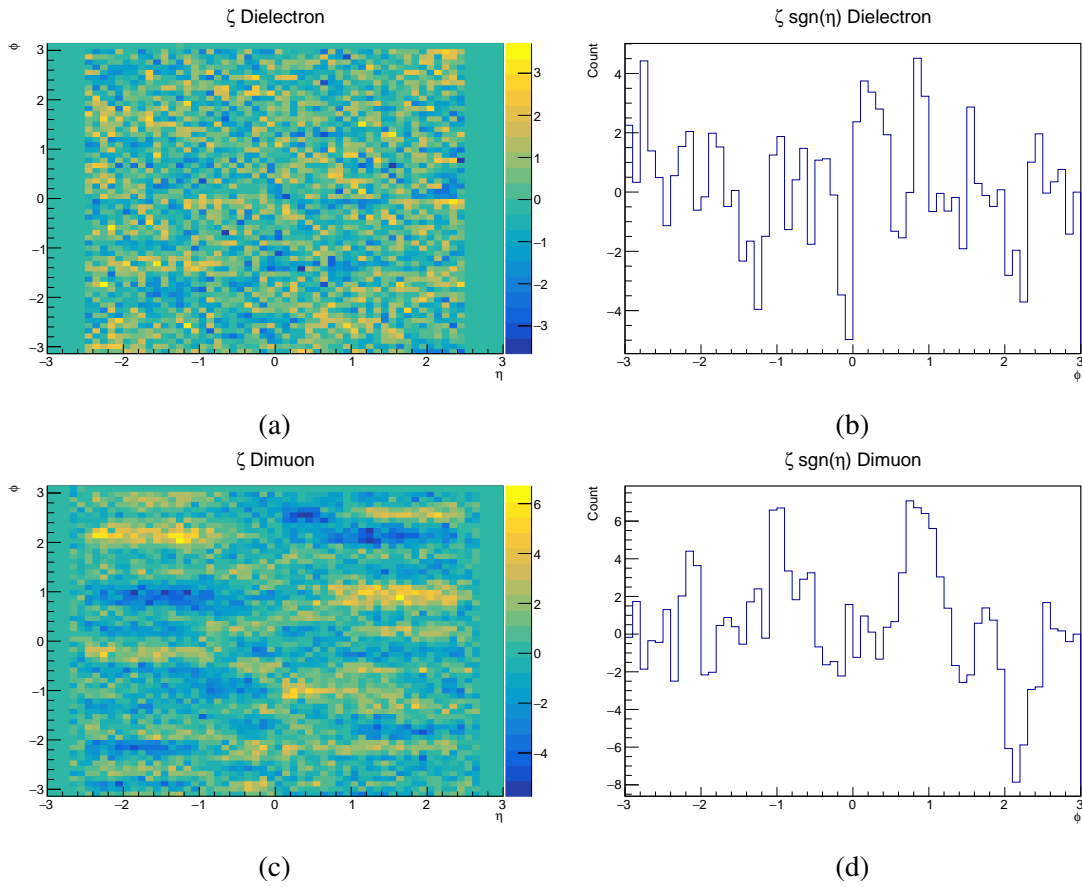


Fig. 3.2 Here we have dilepton ζ plots. 3.2a is ζ over electrons and positrons, while 3.2b is its accompanying ϕ -projection in the η -antisymmetric way described earlier. 3.2c is ζ for muons and antimuons, and 3.2d is its ϕ -projection.

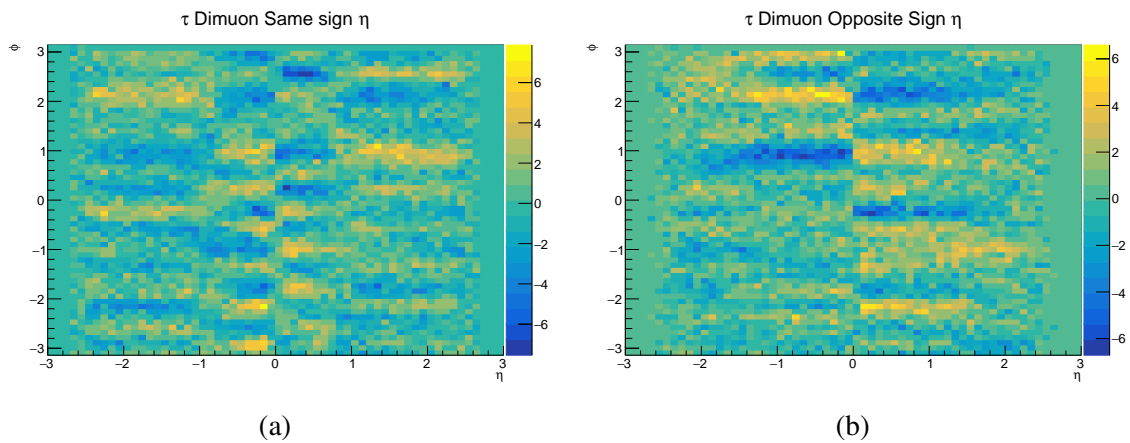


Fig. 3.3 Here we have dimuon τ plots. On the left, we have the normal dimuon τ plot, but we have limited it to events where the leptons have the same sign in η . On the right, we have the reverse, in that we only keep events with opposite signs in η . There is significant, yet different, activity in both plots. Further study is definitely necessary.

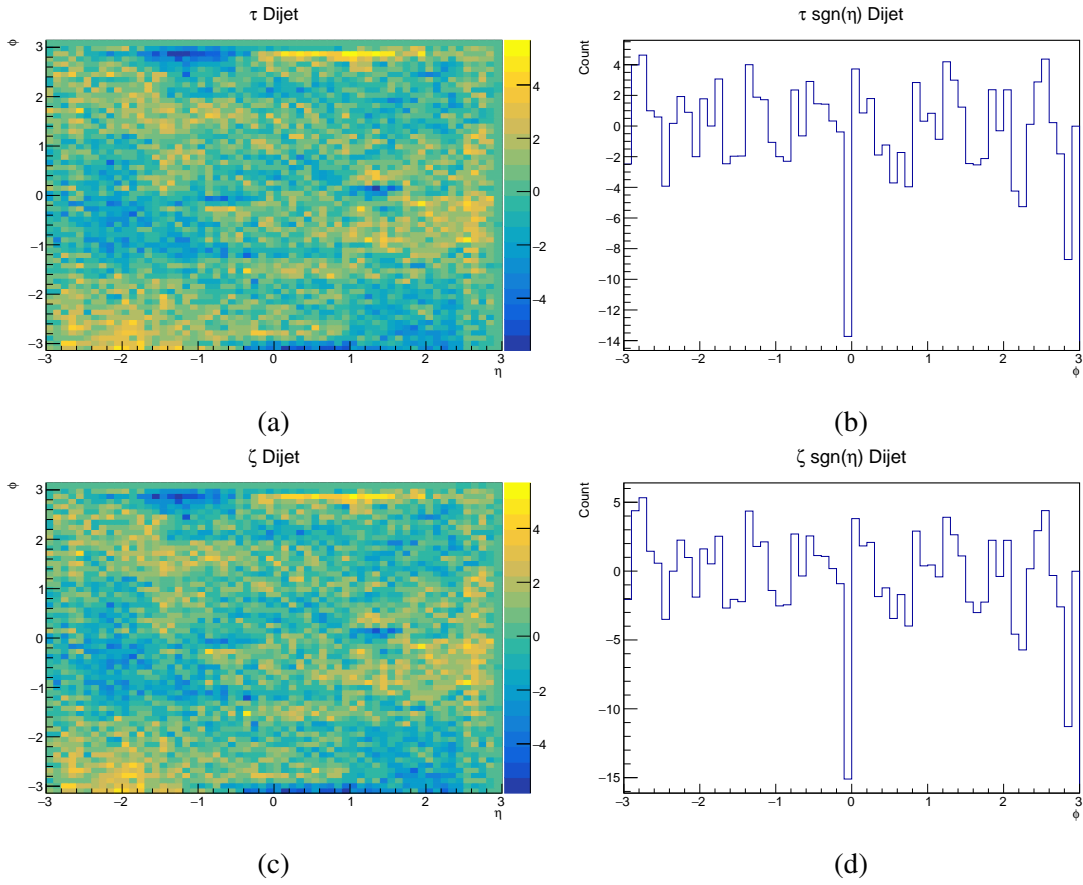


Fig. 3.4 Here we have 3.4a and 3.4c, the τ and ζ plots, respectively, over dijet events. 3.4b and 3.4d are the η -antisymmetric ϕ -projections of τ and ζ respectively.

ζ are bigger than those for τ . In Figure 3.5, we see τ , again plotted for our dijet sample, but where we again restrict the η of jets to be either the same or opposite signs. Now the substructure of Figures 3.4a and 3.4b is much more resolved, with obvious bands in ϕ . We will try to interpret these in chapter 4.

3.2.3 Jet Triad Observable

A plot of Λ for 2017 jets with the previously mentioned cuts is shown in Figure 3.6. Here we choose the order of the jets to be in order of decreasing p_T , but other choices can be made. One can notice the structure building up around $\phi = \pm\pi$, which very well may be related to the similarly prominent structure from the dijet ζ and τ plots, but again, this is speculation. Notice also that, in comparison to the muons plots, there is much less substructure. However, in my opinion, that small structure is worth further study.

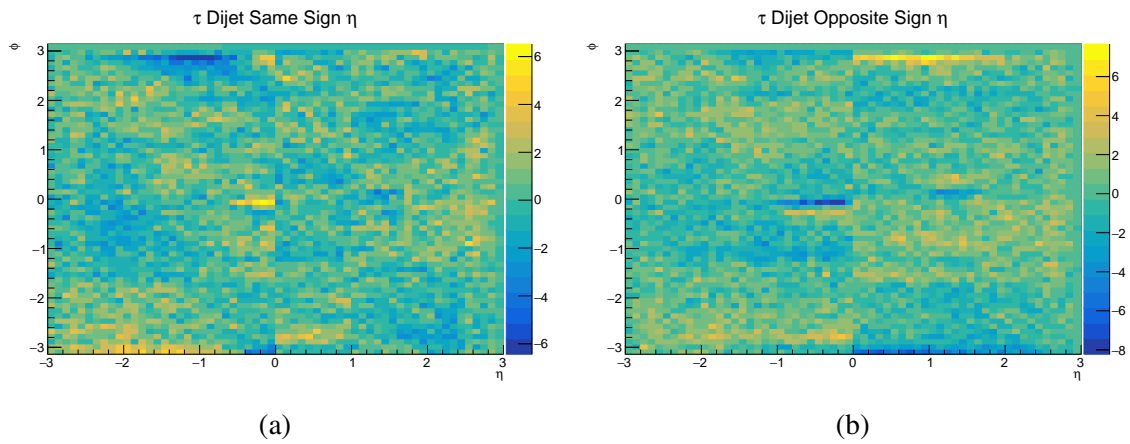


Fig. 3.5 Here we have dijet τ plots. On the left, we have limited it to events where the jets have the same sign in η . On the right, we have the reverse, in that we only keep events with opposite signs in η . There is significant activity in both plots, highlighting interesting structures around $\phi = 0, \pi$.

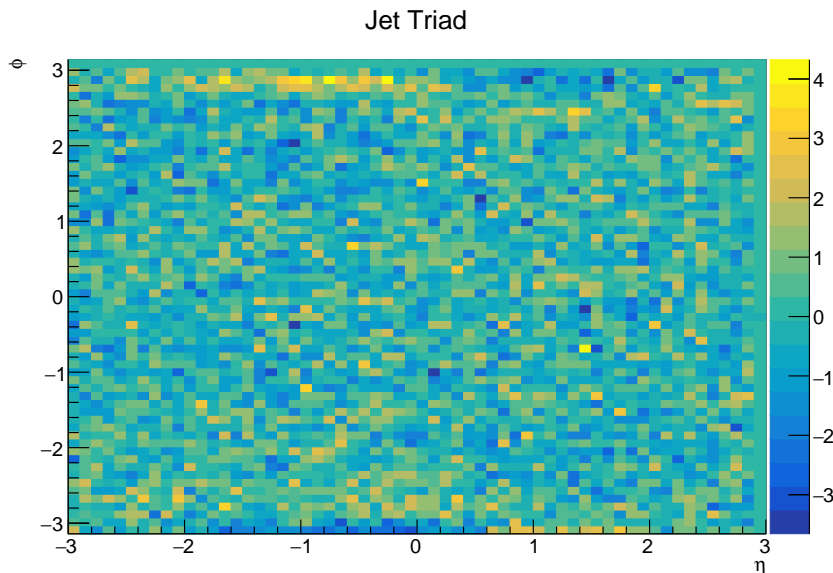


Fig. 3.6 A plot of the jet triad observable, Λ . There is some curious structure at approximately $\phi = \pm\pi$, which is more than likely related to the same structure in the dijet plot, but overall there is much less structure than found for the two jet observables.

Table 3.1 Total parity violation statistic, O_{tot} , for our samples

	τ	ζ	Λ
Dilepton	1.45	2.78	—
Dielectron	0.04	1.16	—
Dimuon	1.97	2.66	—
Dijet	3.38	3.20	—
Trijet	—	—	-0.57

3.2.4 Summed Results

We can also calculate the properly normalized total statistic for the entire plot, or $O_{tot} = \frac{N_p - N_n}{\sqrt{N_p + N_n}}$, for each observable and each sample and whose value is the significance of a global nonzero value for our plot. Shown in Table 3.1 are all of the values of this statistic for our samples. One can see that none are at the 5σ level, leading to the conclusion that the signal in our plots is dominated by local detector effects.

Chapter 4

Parity Violation from the Detector?

4.1 Effects of Weak Modes on Tracks

Clearly spotting a signal in the ATLAS detector in one of our observables does not immediately signal parity violation. In making our previous arguments, we assumed the ATLAS detector was an ideal instrument which was invariant under parity transformation and measured everything with perfect accuracy in the detector. This is not quite the case for many reasons, some of which we have very good control over, and some which we have less good control over. Categorizing all of the things that could possibly go wrong in a machine like the LHC or the ATLAS detector and the work done to combat these possibilities fills volumes of a library. Categorizing things that can go wrong without being completely obvious, like the detector having massive system failure, is an admittedly smaller subset of this, but still a large space. The ATLAS detector and detectors in general reconstruct particles by playing connect-the-dots on recorded energy hits in various regions of the detector along with a possible total energy signature from one of the calorimeters. In the inner detector, where a 2 Tesla magnetic field points parallel to the beam axis, particles curve in the transverse plane with a curvature which scales inversely with the particle's p_T . Many deformations of the detector can be fixed at the software level by laser and other physical measurements before the runs, and when reconstructing particle tracks, many local deformations can be spotted by the failure of particle tracks in that region or even in the detector as a whole to maintain circular shapes. Local and global χ^2 analysis can spot and correct these and other similar deformations in software after the run [20].

A more devious set of deformations and an indeed countable set of deformations which cannot be attacked with this analysis method are the weak modes. These deformations take the curved particle tracks to different particle tracks with approximately circular curvature which cannot be pointed out particle-by-particle in analysis. These types of deformations can

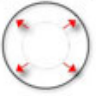

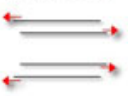
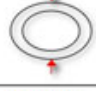

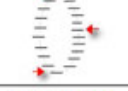


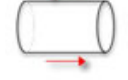
	ΔR	$\Delta\phi$	ΔZ
R	Radial Expansion (distance scale) 	Curl (Charge asymmetry) 	Telescope (COM boost) 
ϕ	Elliptical (vertex mass) 	Clamshell (vertex displacement) 	Skew (COM energy) 
Z	Bowing (COM energy) 	Twist (CP violation) 	Z expansion (distance scale) 

Fig. 4.1 The weak modes of the ATLAS inner detector [1]

systematically bias measurements in regions of the detector by increasing or decreasing the p_T of particles, possibly changing the η and ϕ of a track, and decreasing the signal to noise ratio in measurements. Even more deviously, the increased temperature inside the detector when it is hot can cause these deformations which will be different than when the beam is off. The set of weak modes are categorized using the cylindrical coordinates, $\{r, \phi, z\}$ and induced by warping one direction proportionally to that or another direction in the set. For example, $z \rightarrow z - sz = (1 - s)z$, where s is a dimensionless scale factor defines a linear expansion in z . Similarly, $r \rightarrow r - s \sin \phi$, where s now has dimensions of length introduces an elliptical shape into the detector.

Looking at Figure 4.1 [1], most of the deformations will not affect particles in any way which could possibly introduce a global parity signature, but as particles curve in the magnetic field in a direction which depends on their charge, it appears possible that twists, or $\phi \rightarrow \phi - sz$ could affect the momenta of the particles in a way which could produce a false-positive global parity violation signature. It is also possible that other such deformations could produce local effects like that seen in muons. In order to understand future results of parity-violation, it is important to understand every possible different systematic way parity violation could be falsely introduced.

We derive the effect of twists on particle transverse momenta in Appendix A, but the major result is that

$$p'_T = p_T^0 \left| 1 - \frac{2sp_T^0}{qB} \sinh \eta \right|^{-1} = p_T^0 |1 - 2sv_z^0 D|^{-1} = p_T^0 |2D\varepsilon|^{-1}, \quad (4.1)$$

where s is the twist parameter used in the definition of the twist, q is the particle charge, $B = 2$ Tesla, $D = \frac{m\gamma}{qB}$, where γ is the appropriate Lorentz factor and m is the particle mass, and finally $\varepsilon = \frac{1}{2D} - sv_z^0$, where v_z^0 is the particle's true velocity along the z -axis. This equation relates the transverse momenta of particles in a perfect detector, p_T^0 , to that measured by a detector afflicted with a twist, p'_T as a function of the η of the track.

Thus, we see that the transverse momenta of the particles are altered in a way which depends on the signs of many things, including the charge, the direction of the twist, and the momentum along the beam axis. We also notice something that is a hallmark of this effect. Coming back to ε , we see that when it reaches 0, the particle loses the information of which way the particle curved, and the transverse momentum becomes infinite. If ε continues past 0, the particle's curvature flips direction and begins to decrease in magnitude from infinity. This can turn particles in one η region of the detector into antiparticles while doing the opposite in the opposite η regime, as shown in Figure 4.2. If the initial distribution over particles was η symmetric, this would show up as an over-production of particles in one direction and antiparticles in the other at high enough $|\eta|$, or explicit and unphysical CP violation in the detector. However, the twist would have to be rather large for any effect like this to be measured. While it is indeed interesting that we have pegged this as charge-parity violation, can it also translate to a parity violation signature, or a nonzero mean, in ζ ?

This question is linked with the problem of measuring s from a distribution of particles. One method of attempting to obtain s comes from the p_T distributions of a particle in forward or backwards η . One could use the p_T distributions for particles with a particular reconstructed charge to find s . As is highlighted in [20], and as we have discovered, if we pick a particular η region, then particles are more likely to come out with higher or lower p_T depending on their charge content. The effect can be seen in the construction of the Z invariant mass from the constituent decay into dilepton. If the leptons both enter the forward η region of the detector, then there will be a systematic difference between the positron and electron p_T distributions depending on direction of the twist. If they enter different regions, then this will contribute to noise around the peak corresponding to the Z -mass. Statistical methods focusing on cleaning this peak can spot twists in the detector. Another useful method is the reconstruction of cosmic tracks, as these weak modes depend on the starting point being close to the interaction vertex, so tracks coming from all angles can pinpoint some of these deformations. Cosmic runs however, are less clean and useful when the detector is on and hot, which is especially when extra twists or other weak modes can be introduced.

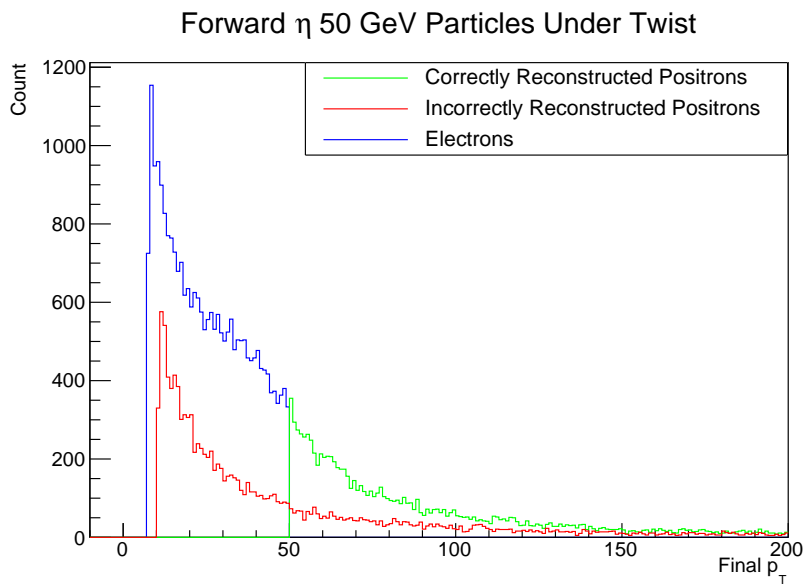


Fig. 4.2 The effect of a $s = 0.003/\text{m}$ twist on 50 GeV particles with positive η . The curvature of electrons gets increased, as they curve in the direction of the twist, so they begin to clump towards 0 GeV. The reason it does not hit 0 GeV in this plot is due to our η cuts. Positrons on the other hand curve in the opposite direction, so their curvature decreases to a straight line with infinite p_T before being misreconstructed as an electron and decreasing in p_T from infinite to 0 GeV. The degree to which this effect is experienced scales with the η of the track, and the effects for positrons and electrons switch when $\eta < 0$.

4.1.1 Effects of Twists in Observables

As we have stated already, because twists can be defined to not change the η_0 or ϕ_0 at the collision point, the variable we defined as τ will be unaffected. Thus, τ is an inherently better observable if one required absolute immunity from twists to be a necessity. However, can we use the apparent twist sensitivity of ζ to highlight twists in the detector, or could twists affect ζ in a way which could mimic parity violation?

I constructed a Monte-Carlo which started with a given set of particles, with their η, ϕ , and p_T taken from the distribution of my leptons data. I could not take exactly the leptons data itself for two reasons: one, twists can change the p_T of particles up as well as down, and if a twist lowered the p_T of a particle below my p_T cuts, that would not work. Also, τ and ζ both showed large bands, which, for this analysis, it would be better to have removed. We will not be comparing these results to experiment, but only extracting any qualitative features seen.

I took the lepton data, fed the necessary track info into distributions to be drawn from, and I set up a series of coaxial cylinders with the radii of the inner detector levels, which are, in mm, $\{50.5, 88.5, 122.5, 299, 371, 443, 514\}$. Then I evolved particles traveling through my inner detector in a magnetic field according to A.8, which was inserted into equations A.3 and A.4 to get the particle coordinates as a function of the inner detector radii. I then implemented a function to change the positions of the points at each level of my inner detector according to a transformation defining the relevant weak mode; for twists, this was $\phi \rightarrow \phi - sz$, but the others were implemented as well. I reconstructed the paths and track data from these points and got a ζ distribution. As a check on the entire Monte-Carlo system, I calculated the altered p_T value from equation A.22 and then plugged this resultant value into equation 4.3 to get the resultant distribution on ζ .

I raised the p_T cut for this test to 50 GeV so as to not bias the result and allow particles from 25 GeV to have their p_T increased by the 0.001/m twist to the cutoff. If a twist brought a particle in my simulated events below my p_T cut, I discarded that event, but otherwise accepted. We see the effect of plotting ζ as in O_1 in Figure 4.3. In the panel on the left, we have plotted our results for $s = 0$, while on the right we have our results for the rather large twist of 0.001/m. We see no effect in either plot.

Looking at ζ , we may wonder how changing the transverse momentum of particles would have any effect on this, as it explicitly depends on the x,y, and z momenta. The solution is that each momentum projection is constructed from the measured transverse momentum and an angle in the detector. We can rewrite ζ in terms of measurable quantities like so:

$$\zeta = (p_{T1}p_{T2} \sin(\theta_2 - \theta_1)) \text{sgn}(p_{T1} \sinh \eta_1 - p_{T2} \sinh \eta_2) \quad (4.2)$$

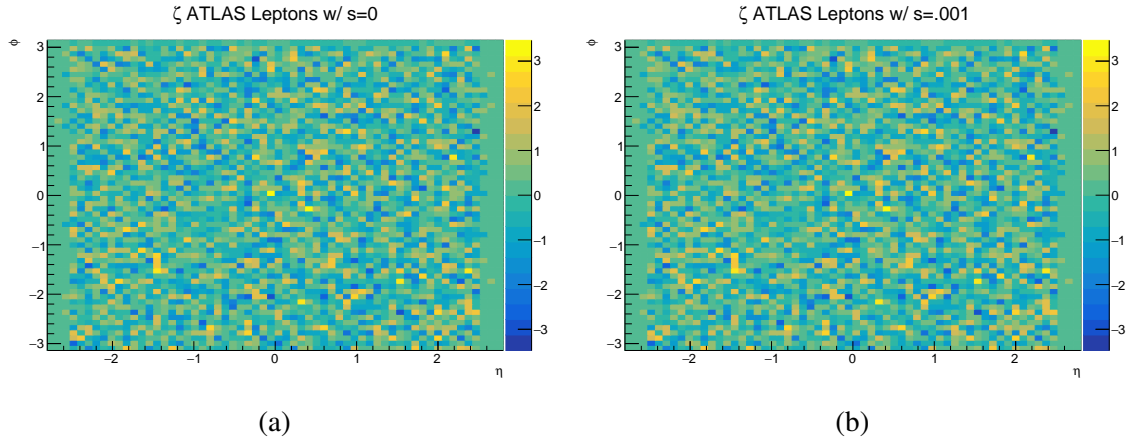


Fig. 4.3 Effect of twists on ζ in our Monte-Carlo

Since θ_1 and θ_2 are measured at $z = 0$, neither of them changes under twists, and even if we were to define $z = 0$ to not be the center of the collision, if the particles collide at the same point on the z -axis, then the difference $\theta_2 - \theta_1$ is still conserved. Of course in reality, all final particles in an event do not come from $x = y = z = 0$. First off there are secondary splittings and hadronization effects which generate the final particles. Hadronization occurs over such a short length scale compared to any actual length scale of the detector that all hard particles effectively come from a very small central region, and as long as we look at the highest p_T particles, then they should carry most of the momentum, preserving, to a good approximation, a worldline which passes through the center of the collision. There is also a spread of the collisions due to beam focusing effects in the detector, as it is impossible to get all the beam particles down to a single point. The less focused beam which is accelerated around the ring is focused such that the collision region for the beam is an ellipsoid Gaussian distribution. In run 1, this ellipsoid had a transverse standard deviation of approximately 13 μm and a longitudinal standard deviation of roughly 54 mm [21]. If we analyze how this could come into play in an observable like ζ , we see that since $\phi \rightarrow \phi - sz$, any deviation in z translates to an extra deviation in ϕ . Specifically, if our two particles have a difference Δz between their collision centers, then this would show up as a factor of $\Delta\phi = s\Delta z$ in the difference of the angles in the transverse plane. Since the collision point on the z axis is Gaussian centered at $z = 0$, then $\langle z_{col} \rangle = 0$, and we know $\sigma_{z_{col}} = 54\text{mm}$, this implies $\langle \Delta z \rangle = \langle z_2 \rangle - \langle z_1 \rangle = 0$ and $\sigma_{\Delta z} = 54\sqrt{2}\text{mm}$. This leads to a standard deviation on the angle difference, $\sigma_{\Delta\phi} = s * 54\sqrt{2}\text{mm}$. If we (very easily) assume that s , for the purposes of getting an order of magnitude estimate, is below $0.003/\text{m}$, then $\sigma_{\Delta\phi} < 2.3(10)^{-4}\text{rad}$. This will not contribute to any visible effects, so we choose to ignore it for the time being.

Thus, we assume twists do not alter $\theta_2 - \theta_1$, and we get that after such a twist,

$$\zeta' = (p'_{T1} p'_{T2} \sin(\theta_2 - \theta_1)) \text{sgn}(p'_{T1} \sinh \eta_1 - p'_{T2} \sinh \eta_2). \quad (4.3)$$

Everything but the signum function is going to come off as unchanged or a strictly-positive multiplicative correction, so it will not change the overall sign. We focus on the signum function:

$$\text{sgn}(p'_{T1} \sinh \eta_1 - p'_{T2} \sinh \eta_2) = \text{sgn}(p_{z1} \left| 1 - \frac{2sp_{z1}}{q_1 B} \right|^{-1} - p_{z2} \left| 1 - \frac{2sp_{z2}}{q_2 B} \right|^{-1}) \quad (4.4)$$

Clearly there are nontrivial effects which can alter the sign of this signum function, but from this we can see that twists cannot induce a parity signature in ζ separate from anisotropy, as the $\sin(\phi)$ is just along for the ride under twists, and is not affected. This answers our second question; effects associated with twists of the inner detector probably do not produce this banded structure present in the plot for τ . Could they produce the apparent anisotropy, and what other constraints are there on any anisotropy produced? First, there is the problem of the CP nature of the twist. The two observables upon which every other observable which is changed by twists is built are p_T and q . p_T transforms according to equation A.22, with a factor of $\left| 1 - \frac{2sp_T^0}{qB} \sinh \eta \right|^{-1}$, while q transforms with the sign of that, or in other words,

$$q' \rightarrow q \frac{1 - \frac{2sp_T^0}{qB} \sinh \eta}{\left| 1 - \frac{2sp_T^0}{qB} \sinh \eta \right|}. \quad (4.5)$$

However, every factor of η in either is directly multiplied by q for the particle. We can then construct an observable out of these two things and other things which may or not depend on them to produce an arbitrary observable, which we can also enforce is odd under $\eta \rightarrow -\eta$. If we are to sum over all charge pairs of lepton-leptons, the greater majority of the events will be particle-antiparticle, and the rest will be particle-particle and antiparticle-antiparticle, but these last two will be both small in number and not even only because of the small tendency for more positive than negative charges in these events. The overall consequence is that any observable, with all charge combinations summed over in their proper ratios will leave no room for $\eta \rightarrow -\eta$ to change the sign, as every term with $-q$ in the transformation for particle 1 will just flip signs with another term which has q in its transformation, and so on for all the combinations. This means the anisotropy cannot be produced either, as our data included all charge combinations.

So what are twists doing to ζ , if anything? To see that, let us define one last plotting method for our observables. We simply plot the number of positive minus the number of negative results for the observable, but this time we will bin over $\Delta\phi$ and $\Delta\eta$ for the two leptons in the event. Both two-particle observables have a nonzero expectation value everywhere on this plot even in the ideal detector case and with no parity violation; taking τ as an example, $N_p(\Delta\phi, \Delta\eta) - N_n(\Delta\phi, \Delta\eta) = N(\Delta\phi, \Delta\eta) \frac{\tau(\Delta\phi, \Delta\eta)}{|\tau(\Delta\phi, \Delta\eta)|}$. ζ has a slightly different behavior in these types of plots, as we will soon see, but this is a very accurate approximation if the transverse momenta of the two particles are close and the detector can be assumed to be ideal. In conclusion, there is no appropriate normalization, so in order to eliminate the arbitrary dependence of the plot's color scheme on the number of events in the bin as well as the arbitrary dependence of the frequency of different $\Delta\eta$ and $\Delta\phi$ values in Monte Carlo, we will divide by the number of events which go in the bin, even though now it does not mean any error on the plot. This will make the color scale range from $\{-1, 1\}$. This results in

$$O_3(\Delta\phi, \Delta\eta) = \frac{N_p(\Delta\phi, \Delta\eta) - N_n(\Delta\phi, \Delta\eta)}{N_p(\Delta\phi, \Delta\eta) + N_n(\Delta\phi, \Delta\eta)}. \quad (4.6)$$

We plot ζ from our constructed lepton distributions at the top of Figure 4.4. We see 4 colored corners, which match the same colors that a plot of τ with this method would have. The hole in the middle comes from two leptons not being allowed to be literally on top of each other, or their tracks could not be distinguished. The interesting thing is the noise around the $\Delta\eta = 0$ line. We can see where this comes from in the following two figures. Figure 4.4b plots ζ assuming the p_T values are the same for a twist parameter $s = 0$, and for simplicity, that the η and ϕ distributions are flat. Figure 4.4c does the same, but it assumes the original particles had the same p_T before the 0.003/m twist. The twist is mixing up the p_T of the particles in the event, but this is being hidden under the fact that the particles are already very well mixed in terms of p_T . Any effect in our observable will simply be drowned out by the different momenta.

One last thing before we move on. As we mentioned earlier these observables were motivated from what we believe are good properties that any parity sensitive observable should have. We mentioned that we could add in components which do not ruin the overall symmetries, and here we explore that. The easiest example to see is Λ . As defined, it depends on the transverse momenta of all 3 particles on which it depends, but without affecting any of the symmetries, we could just divide all of these transverse momenta out, and the resultant observable would now no longer depend on the transverse momenta, and thus would receive no corrections from twists. A slightly subtler example is that of ζ . Under twists, $p_T \rightarrow p_T |2D\mathcal{E}|^{-1}$, and combined with equation 4.5, this means that $\frac{p_T}{q} \rightarrow \frac{p_T}{q} (2D\mathcal{E})^{-1}$ and

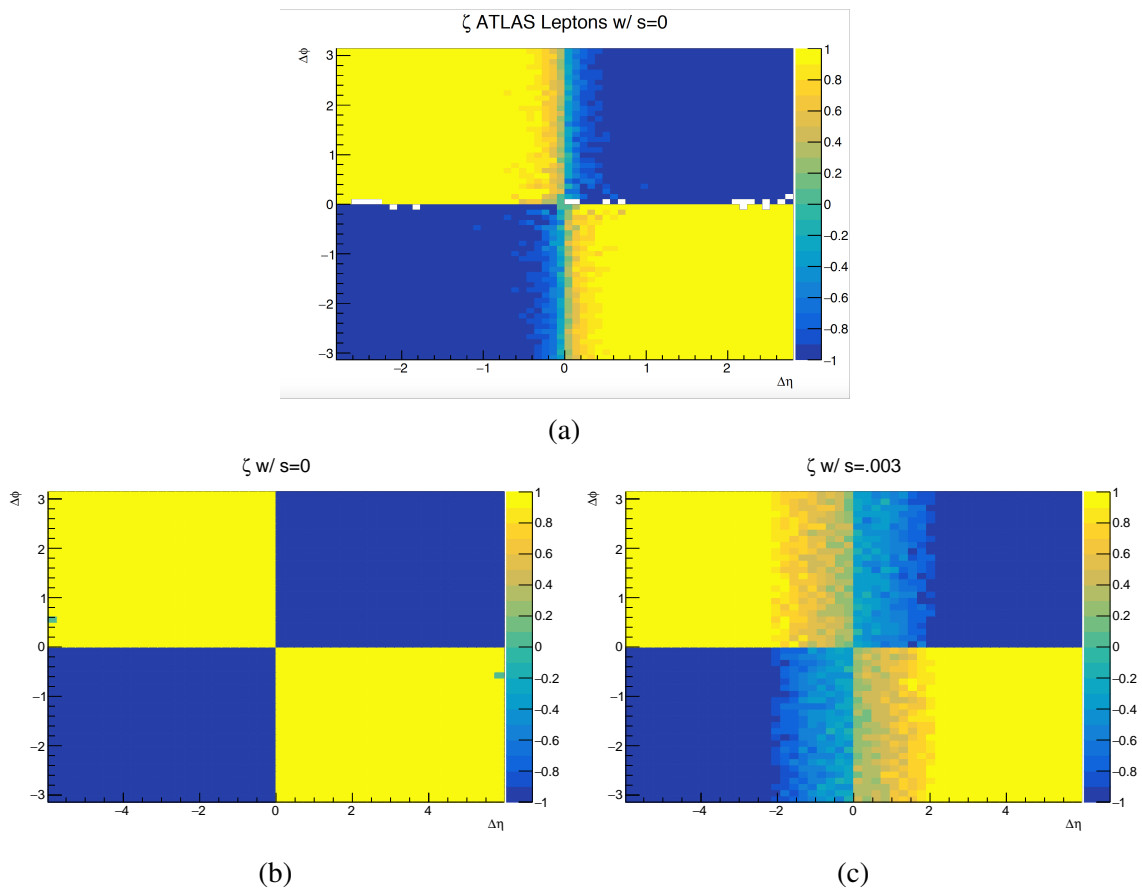


Fig. 4.4 The effect of twists on ζ plotted as a function of $\Delta\eta$ and $\Delta\phi$

thus that

$$\frac{p_{z1}}{q_1} - \frac{p_{z2}}{q_2} \rightarrow \left(\frac{p_{z1}}{q_1} \left(1 - \frac{2sp_{z2}}{q_2 B} \right) - \frac{p_{z2}}{q_2} \left(1 - \frac{2sp_{z1}}{q_1 B} \right) \right) \left(1 - \frac{2sp_{z1}}{q_1 B} \right)^{-1} \left(1 - \frac{2sp_{z2}}{q_2 B} \right)^{-1} \quad (4.7)$$

The big parenthesis cancels down to $\frac{p_{z1}}{q_1} - \frac{p_{z2}}{q_2}$, leaving only the two factors on the right. If we use this construction instead of Δp_z in ζ , the sign of these two terms can exit the signum function and when multiplied by the $|2D\varepsilon|^{-1}$ terms from the p_T factors outside the signum function, make it so that

$$\zeta \rightarrow \zeta \left(1 - \frac{2sp_{z1}}{q_1 B} \right)^{-1} \left(1 - \frac{2sp_{z2}}{q_2 B} \right)^{-1} \quad (4.8)$$

Alternatively, we can just forget all of the factors of p_T such that $\zeta = \sin(\theta_2 - \theta_1) \text{sgn}(\sinh \eta_1 - \sinh \eta_2)$, something very close to τ and completely invariant under twists. As we can see, even when we have an idea of the scope of observables from symmetry arguments, small changes can greatly impact how observables interact with various detector effects.

4.1.2 Effects of Other Weak Modes on Tracks

With this example under our belts, the rest of the weak modes are just as, if not more understandable. Referring back to Figure 4.1, there are 8 other weak modes to consider with various different s values with different dimensions. Radial expansion, or $R \rightarrow R - sR = (1 - s)R$, and Z expansion, or $Z \rightarrow Z - sZ = (1 - s)Z$, both simply put a multiplicative factor on their relative dimensions. Radial expansion for example, will mostly only change the interaction vertex. Z expansion will mostly just change the η for each track [20].

The math behind curls is very similar to that of twists. In fact, the difference comes in equation A.12, where we instead get $\phi' = \phi - sr$. With the knowledge that t , or the time the particle has traveled along its track, is small for our tracks in equation A.7, as shown in the appendix, we get that $r(t) = \sqrt{2D}v_T \sqrt{1 - \cos \frac{t}{D}} \approx \sqrt{2D}v_T \sqrt{\frac{t^2}{2D^2}} = v_T t$, so ε for curls just doesn't include the factor of $\sinh \eta$, and the rest of the derivation proceeds the same, such that $p'_T = p_T^0 \left| 1 - \frac{2sp_T^0}{qB} \right|^{-1}$. While this no longer links C and P, it just doesn't include P anymore, so it isn't as interesting for our purposes.

We saw that there was very visible band structure in ϕ in the muons τ and ζ plots. The middle row of the weak modes table looks like it could maybe produce some of this structure. Since these particular effects were in both τ and ζ , we will now just focus on their effects on τ . An elliptical deformation, or $r \rightarrow r - s \sin(\theta)$ does not pick an η direction, and

as $\theta \rightarrow \arctan\left(\frac{r' \sin \theta}{r' \cos \theta}\right) = \arctan \tan \theta = \theta$, there is no change in the transverse orientation between the particles after. If τ starts flat, it ends flat.

Clamshells, which are defined in the top half plane by $\phi \rightarrow \phi + s(\pi/2 - \phi)$ and $\phi \rightarrow \phi + s(-\pi/2 - \phi)$ in the bottom half plane, where $0 < s < 1$, can show signals of parity violation. While the detector will have holes in the "mouth" of the clam, as the panels bunch around the "top" and "bottom" shell as in Figure 4.5, in order for this transformation to be a weak mode, it will happen in such a way that the ratio between two different areas in the top half plane before and after the transformation will not change, so there will be no signal for a completely even and uncorrelated distribution of particles in $\eta\phi$, as shown in Figure 4.5a. In this and the following figures, since p_T distributions are not important for τ , we simply assume an even distribution over $\eta\phi$ for the purposes of extracting the features of the τ plot, to which we apply our clamshell. If we limit the correlations between the particles in the event in a simple way, particles which tend to be back-to-back with their counterpart in ϕ and which fall near the border of the cut-off region can have the distribution of their second particle cut off by the clam opening. This would make $\Delta\phi$ tend to choose a particular sign and introduce color in our plots for events on the border of the clamshell as shown in Figure 4.5b, which is taken over all particles with $|\Delta\phi| > (\pi - 0.5)$. A similar effect happens when we switch gears to $|\Delta\phi| < 0.5$ in Figure 4.5c.

Since the clamshells in the top and bottom of the defining figure are effectively separate structures, they could also have different s values, and this would bring visible systematic differences. For example, one can see from the transformation property of the clamshells and equation A.12 that the math behind this transformation's effect on p_T will be exactly the same as twists except that $\varepsilon = \frac{1-s}{2D}$ this time, and equation 4.1 will combine for $p'_T = \frac{p_T}{|1-s|}$. This would make a different p_T distribution for either half of the space, which could be distinguished if the effect were large enough, not to mention the particle density will be lower as well.

The last of this middle row is the skew transformation, or $z \rightarrow z - s \sin \phi$, which, indeed, would not have much of an effect on any given plot of our observables if there were no inter-particle correlations, and neither would it affect p_T in any way, as the $r\phi$ information is preserved. However, let us assume we have a set of dilepton events which come from either a highly boosted Z or a two- Z production, which thus deposit their leading particles within a small $\eta\phi$ range. Let us imagine a region which does not include the critical points where the skew direction begins to change. Thus, if our first binned particle lands at a particular ϕ within this region, the skew will change our circle in $\eta\phi$ into an ellipse which picks either increasing η with increasing ϕ or increasing η with decreasing ϕ , and the other region separated by the critical points will get the other. Thus our points will tend to lie in a region

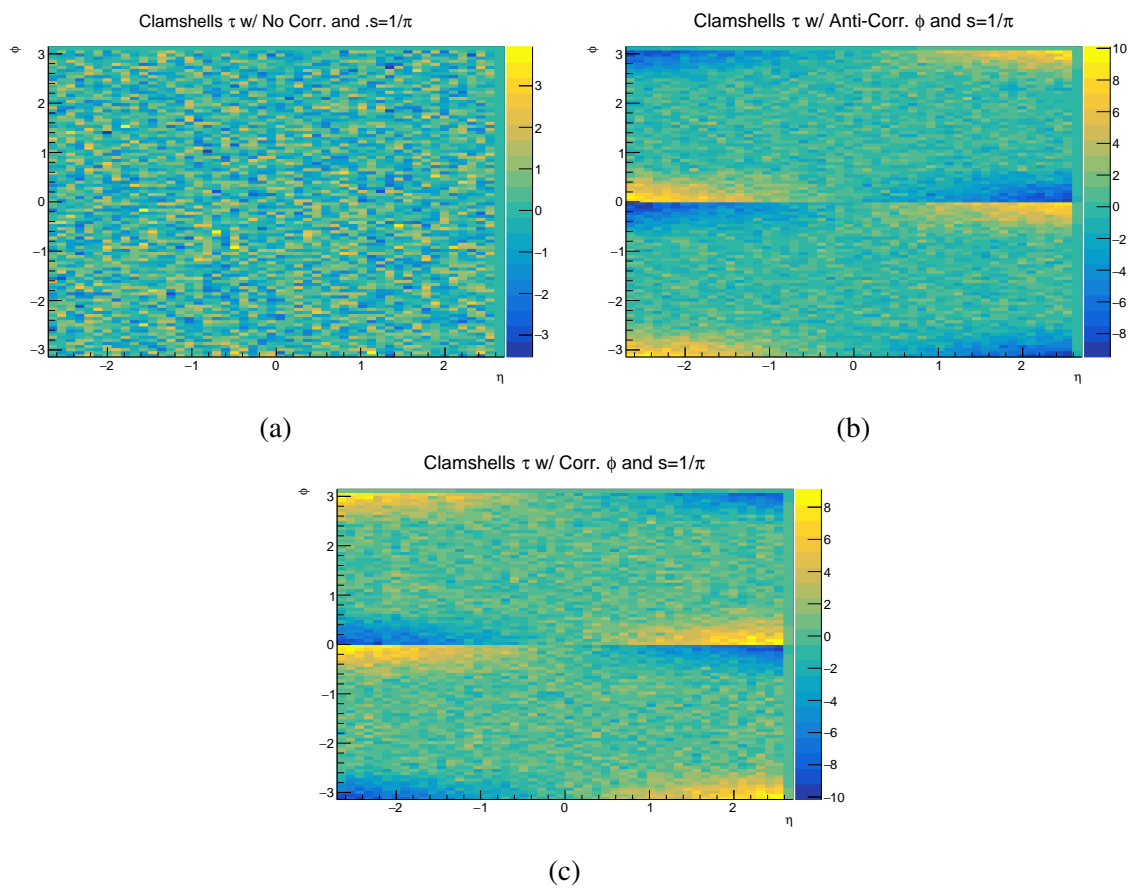


Fig. 4.5 A sample of the possible effects of clamshell deformations on τ from Monte-Carlo

which picks a local handedness until the critical point, and then the opposite handedness can be preferred if the direction of skew changes. The same logic applies when the particles tend to be back-to-back instead, and the sign of the observable will be picked by the direction of skewness in the region opposite the first bin.

4.2 Detector Inefficiencies

Alignment issues are far from the only issue that could and do plague the ATLAS detector. Another broad class is that of detector inefficiencies, or the failure of sections, pixels, tiles, or any similar structure in the detector to reliably record when a relevant particle comes through. This does not count failing to detect a particle which the section is not designed to perceive, as no part of the detector can measure neutrinos and some pieces, like the TRT are designed to not measure muons. If for example, sections of the inner detector were to flat-out stop measuring particles due to severe radiation damage, age, or any number of other reasons, then this must be known so it does not bias statistics. While not as severe, a section of the detector could measure a particle hit only a certain percentage of the time, or a calorimeter could only record a fraction of the energy deposited at the place for some similar reason. All of these occurrences happen constantly, and monitoring this is one of the main jobs during the run, or otherwise massive statistical noise can be introduced from what was once good signal. On the other hand, in terms of what we are looking at, it can produce signal out of pure noise. Let us look at some examples.

In these examples, we will just look at our τ observable, as the measured p_T of the particles will not come into play here. In truth, since the ATLAS Muon Spectrometer is designed such that every muon will pass three different layers for a measurement of the curvature in the outer detector's magnetic field, the likelihood is that hits may not be recorded or something similar before entire $\eta\phi$ regions of the detector suddenly stop working. If sections of a layer become inefficient or go silent, then momentum measurements will also suffer and possibly change, but we will disregard that for the purposes of this exercise. We will also assume a flat distribution over η and ϕ as well as no correlations between our particles, for our illustrative purposes. Thus, there should be no signal above noise that our detector sees in τ .

First, imagine the ATLAS detector loses the ability to detect particles in $|\phi - 1| < \pi/50$. This is a large region for pure viewing purposes, but indeed it is only 1 percent of the ϕ coverage. We can see the result in Figure 4.6a, where τ in this poor detector is plotted on η vs ϕ . We can see that obvious structure has resulted from this hole. Why does this exact structure arise? Imagine our first particle gets binned in forward η and at slightly higher ϕ

than the hole. $\Delta\eta$ is already more likely to be positive, but now $\Delta\phi$ has more area of the detector where it will be negative, as a section just below is missing. When the negative sign in the definition of τ is added, this comes out to the yellow region shown. The other regions follow a similar logic. Notice that singling out the line at $\phi = 1$ also singles out the line at $1 - \pi$, because this is the very ϕ value at which our previous argument breaks down. There is equal area "above" and "below" the line as $\phi = 1$ is the border.

This seems maybe a little bit extreme to assume 1 percent of the detector, organized in such a fashion is silent or tending to be silent. What about something more sane, like a patch of the detector? Shown in Figure 4.6b, we can see what would happen if this patch were a circle in $\eta\phi$ of radius 0.2. The resultant shape is very similar for the same reason as before. There is already a $\Delta\eta$ preference when the first particle's η is chosen, but the hole's ϕ position induces a preferred value of $\Delta\phi$ just like before, which colors the plot.

One more possible interesting shape is one which does not bias ϕ in the same global way. In Figure 4.6c, we see what would happen if the line $\phi-\eta=1$ with a small thickness were removed. In this figure more complicated behavior results, and this time, as we have not singled out a particular ϕ value, but a line in the plane, there is no particular direction in η singled out, and the color pattern is symmetric about the line.

It does indeed appear that this could be a major component of either half of the dilepton τ plots shown in Figure 3.3. These plots show very apparent asymmetry in η , as well as the block type patterns seen in either Figure 4.6a or Figure 4.6b, albeit with much smaller blocks naturally. And much more likely in the detector is not that no signal is seen in a particular region, but that parts of the detector in that $\eta\phi$ regime are radiation damaged such that they produce bad tracks or tracks with too few points from time to time. These areas of the detector can be modeled as accepting a valid track in that regime with some non unity probability, which would also produce this effect, albeit a bit scaled down.

4.3 Theories and Speculations

There are indeed other possible sources of these effects. In leptons, these massive parity violation signatures show up just in muons, and most of these are dimuon events which tend to be back-to-back in ϕ . But some of them have much smaller $\Delta\eta$ and $\Delta\phi$ values. While there are effects in jets which warrant much of our discussion of the whole detector, jets deposit energy and interact with the inner detector, the hadronic calorimeter, the muon spectrometer, the TRT, and really any part of the detector, so full theorizing and positing more specific sources for the signal in those plots is a much more involved job. The fact that the muons produce such clear signal points to the idea that the muon spectrometer may be integrally

involved. Simulating all possible sources, like the systematic deviations in fringe magnetic effects is also very laborious and impossible in exact detail.

But let us look at the dimuon plots for more inspiration. Looking more specifically at the plot for muons which share the same η regime in Figure 3.1d, one cannot help but notice the two regimes, one with $|\eta|$ lower than about 0.8 and the other for $|\eta|$ greater than that. One should also notice the regular banded structure in ϕ . This almost traces out something like the muon MDT system, which functions to track the muons at three separate points in a magnetic field such that the curvature scales inversely with the total momentum of the track. This system is aligned by lasers and in software which attempts the local χ^2 analysis mentioned before, but the alignment precision in the endcap regime ($1.05 < |\eta| < 2.7$) as of 2011 was $110 \mu\text{m}$ [7], and as of 2016 was somewhere between 30 and $60 \mu\text{m}$ with a design spec of $40 \mu\text{m}$ [16].

The system is composed of panels which are layered in order that there are no gaps where muons could sneak through without being recorded. If we have two muon tracks which are close enough to be on neighboring panels, then if each of the panels were moved up or down compared to its neighbors, like, for example, a panel in the direction of positive η is moved towards negative η , then if we binned on the first particle, the ones on the other panel would tend to be in lower η and higher ϕ , making τ and ζ in this region positive. Likewise, if we were to bin on the other particle on the other panel, the first particle would tend to be in higher η and lower ϕ , so τ and ζ are again positive. One could imagine each of the colors in the regime of $0.8 < |\eta| < 2.7$ could conceivably signal small relative shifts in the panels. The same picture results in the much more likely occurrence that the muons are back to back in ϕ , but now panels on opposite sides of the detector can be correlated. Of course one panel being moved does not change the entire η , but small shifts of some of the layers of the muon spectrometer could conceivably lever arm the fit of η for combined inner detector and muon spectrometer tracks. Whether this actually occurs or not is a question for further study.

For events in the next plot where the muons are constrained to have opposite sign η values, that is a much more interesting question. These rather pronounced peaks mean there are correlations for muons which go completely opposite ways in the detector. Since we have chosen the sign of $\Delta\eta$ with the η of the binned particle, and since these muons are highly likely to be back-to-back in ϕ , and thus centered around the π and $-\pi$ border, it is likely that these peaks point not to anything happening at that region of ϕ but to shenanigans in the detector making it more likely that particles around $\phi - \pi$ are likely to go one way from that angle than the other, coloring the entire ϕ band in an η -antisymmetric way.

Chapter 5

Conclusion

In summary, we have performed an analysis of the presence of parity violation in the ATLAS detector, where we explicitly do not make reference to any spin information. We have argued for the validity of our two sets of observables, the two-particle observables, τ and ζ , and the three-particle observable, Λ , from basic principles and measurement considerations, and we recorded the signal of this parity violation in different regions of the ATLAS detector over each of our observables. None of the observables recorded a global parity violation signature above 5σ , pointing to the lack of such a signature being the result of a physical mechanism in the interaction over the entire detector; however, higher statistics over more years may indeed conclude at a later date that such a signature is present. However, there were significant, and very ordered bands, appearing in an approximately η -asymmetric pattern in the dijet and especially in the dimuon samples, while a less significant, but noticeable structure was present in the jet triad observable; this points to systematic effects in the detector as the cause of such a signal. We presented different weak modes of the inner detector, arguing for which ones could produce such η -asymmetric bands, and we also pointed to various detector inefficiency patterns which could be the root cause. The dimuon signal especially, with its different structure inside and outside of $|\eta| \approx 0.8$, coupled with the complete lack of signal in the accompanying dielectron plot, strongly points to different detector effects in the muon spectrometer, which we discussed.

Thus, we come to the very nice speculation that this observable lets us see the detector in a possibly new way! Whether our signals be local alignment issues, detector inefficiencies, an issue in software, or none of the above, there are many more moles to be whacked before any validation of BSM physics can be definitively proclaimed. As it stands, there is no definitive evidence for BSM parity violating effects in our observables, but much signal to be explained.

References

- [1] Muge K Unel and Carlos Escobar. The alignment of the heart of the atlas detector is getting ready for operation phase. URL http://atlas-service-enews.web.cern.ch/atlas-service-enews/2007-8/features_07-8/features_alignment.php.
- [2] Krishna Myneni. Symmetry destroyed: The failure of parity, Dec 1984. URL <https://www.hep.ucl.ac.uk/~nk/teaching/PH4442/parity-violation.html>.
- [3] Karolos Potamianos. The upgraded Pixel detector and the commissioning of the Inner Detector tracking of the ATLAS experiment for Run-2 at the Large Hadron Collider. *PoS, EPS-HEP2015:261*, 2015.
- [4] Commissioning of the ATLAS Muon Spectrometer with Cosmic Rays. Commissioning of the ATLAS Muon Spectrometer with Cosmic Rays.
- [5] G. Aad et al. The ATLAS Inner Detector commissioning and calibration. *Eur. Phys. J.*, C70:787–821, 2010. doi: 10.1140/epjc/s10052-010-1366-7.
- [6] Nikiforos Nikiforou. Performance of the ATLAS Liquid Argon Calorimeter after three years of LHC operation and plans for a future upgrade. In *Proceedings, 3rd International Conference on Advancements in Nuclear Instrumentation Measurement Methods and their Applications (ANIMMA 2013): Marseille, France, June 23-27, 2013*, 2013. doi: 10.1109/ANIMMA.2013.6728060.
- [7] E. Diehl. Calibration and Performance of the ATLAS Muon Spectrometer. In *Particles and fields. Proceedings, Meeting of the Division of the American Physical Society, DPF 2011, Providence, USA, August 9-13, 2011*, 2011.
- [8] Matthew D. Schwartz. *Quantum Field Theory and the Standard Model*. Cambridge University Press, 2014. ISBN 1107034736, 9781107034730. URL <http://www.cambridge.org/us/academic/subjects/physics/theoretical-physics-and-mathematical-physics/quantum-field-theory-and-standard-model>.
- [9] Non-conservation of parity. URL <http://hyperphysics.phy-astr.gsu.edu/hbase/quantum/parity.html>.
- [10] R. P. Feynman and M. Gell-Mann. Theory of the fermi interaction. *Phys. Rev.*, 109:193–198, Jan 1958. doi: 10.1103/PhysRev.109.193. URL <https://link.aps.org/doi/10.1103/PhysRev.109.193>.
- [11] Georges Aad et al. Measurement of the forward-backward asymmetry of electron and muon pair-production in pp collisions at $\sqrt{s} = 7$ TeV with the ATLAS detector. *JHEP*, 09:049, 2015. doi: 10.1007/JHEP09(2015)049.

-
- [12] Zachary R Hulcher and Christopher Lester. private communication, Jul 2018.
- [13] Sophie Renner. *Parity violating observables for LHC searches for new physics*.
- [14] Thomas Gillam. *Summary of 1st year work, including searches for parity violation and R-parity violating supersymmetry*.
- [15] B. H. Brunt. *Searches For New Physics With The ATLAS Experiment*. PhD thesis, University of Cambridge, 2018.
- [16] Georges Aad et al. Muon reconstruction performance of the ATLAS detector in proton–proton collision data at $\sqrt{s} = 13$ TeV. *Eur. Phys. J.*, C76(5):292, 2016. doi: 10.1140/epjc/s10052-016-4120-y.
- [17] Alessandro La Rosa. The ATLAS Insertable B-Layer: from construction to operation. *JINST*, 11(12):C12036, 2016. doi: 10.1088/1748-0221/11/12/C12036.
- [18] Tagging and suppression of pileup jets with the ATLAS detector. Technical Report ATLAS-CONF-2014-018, CERN, Geneva, May 2014. URL <https://cds.cern.ch/record/1700870>.
- [19] Matteo Cacciari, Gavin P. Salam, and Gregory Soyez. The anti- k_t jet clustering algorithm. *JHEP*, 04:063, 2008. doi: 10.1088/1126-6708/2008/04/063.
- [20] Study of the systematic effects induced on tracking 1 by the ATLAS Inner 2 Detector alignment. Technical Report Draft version ATLAS-CONF-20YY-NNN, CERN, Geneva, Feb 2012.
- [21] Morad Aaboud et al. Reconstruction of primary vertices at the ATLAS experiment in Run 1 proton–proton collisions at the LHC. *Eur. Phys. J.*, C77(5):332, 2017. doi: 10.1140/epjc/s10052-017-4887-5.

Appendix A

Twists in the Inner Detector

A.1 Charged Relativistic Particles in Magnetic Fields

In order to have the relevant equations listed, let us do a review of the dynamics of relativistic charged particles in a static uniform magnetic field pointing in the $\hat{\mathbf{z}}$ direction. From the Lorentz force law for this case:

$$\frac{d\mathbf{p}}{dt} = q\mathbf{v} \times \mathbf{B} \quad (\text{A.1})$$

where \mathbf{p} is the relativistic momentum $m\mathbf{v}\gamma(|\mathbf{v}|)$, q is the particle's charge, t is the coordinate time, \mathbf{v} is the particle velocity, and $\mathbf{B} = B\hat{\mathbf{z}}$ is the magnetic field in the inner detector.

For x and y parameterizing p_T and z pointing down the beamline, this differential equation reduces to 2 coupled differential equations and one trivial one:

$$\frac{dv_x}{dt} = -\frac{qv_y B}{m\gamma} \quad \frac{dv_y}{dt} = \frac{qv_x B}{m\gamma} \quad \frac{dv_z}{dt} = 0. \quad (\text{A.2})$$

The last equation is trivial, so we focus on the first two, dividing them and then integrating produces that $v_x^2 + v_y^2$ is a constant of motion for the system, which means the particles are confined to circles in the transverse plane and travel linearly in z . Nothing magical here yet. Since we now know $|\mathbf{v}|$ is constant, this means γ is constant and parameterizing the system is as simple as integrating twice. We summarize the parameterization here:

$$x = D \left(v_x^0 \sin \frac{t}{D} + v_y^0 \left(\cos \frac{t}{D} - 1 \right) \right) \quad (\text{A.3})$$

$$y = D \left(v_y^0 \sin \frac{t}{D} - v_x^0 \left(\cos \frac{t}{D} - 1 \right) \right) \quad (\text{A.4})$$

$$z = v_z^0 t \quad (\text{A.5})$$

$$D = \frac{m\gamma}{qB} = \frac{1}{\omega} \quad (\text{A.6})$$

where v_x^0 , v_y^0 , and v_z^0 are the initial velocities of the particle in the lab frame, and we use D for the inverse of the angular frequency of the circle which the particle traces in the transverse plane as defined above.

Other relations which we derive which will prove useful are that for r , the radius of the particle from the beam axis at $x = y = 0$ and v_T the transverse velocity,

$$r(t) = \sqrt{2} D v_T \sqrt{1 - \cos \frac{t}{D}} \quad (\text{A.7})$$

$$t(r) = D * \text{Acos} \left(1 - \frac{r^2}{2D^2 v_T^2} \right). \quad (\text{A.8})$$

In order to simulate the path of the particles, we can plug equation A.8 into equations A.3 and A.4 to get a parameterization of the particle paths at the inner detector radii.

Once we have this parameterization of the particle paths, and we have simulated evolving the particles according to it in a detector, we will want to modify the particle paths according to our definition of twists, but more on this in chapter 4. Once we have done whatever we want to do to our paths in Monte Carlo, we want to reconstruct the transverse momentum of the particles, which we do by fitting the modified paths of the particles in the transverse plane to circles. The true fit in the detector is done using the sagitta of the circular arc, but we do not need that for our purposes. The idea of weak modes is that new tracks under these transformations should greatly approximate circles, and we will see how exact this is for twists.

A.2 Effects of Twists on Curved Tracks

Here we want to analytically calculate what will happen to the curvatures of the particles' paths through the detector, and thus what will happen to the measured transverse momentum with the addition of a twist.

To make math easier, and because the system is rotationally invariant in x-y, we can take an emitted particle to be emitted in the x direction with no y momentum. Thus, equations A.3 and A.4 turn into

$$x = Dv_x^0 \sin \frac{t}{D} \quad (\text{A.9})$$

$$y = Dv_x^0 \left(1 - \cos \frac{t}{D}\right). \quad (\text{A.10})$$

Thus the angle, ϕ , of the particle with time is

$$\phi = \text{Atan} \left(\frac{D(1 - \cos \frac{t}{D})}{D \sin \frac{t}{D}} \right) = \frac{t}{2D} \text{ mod } \pi. \quad (\text{A.11})$$

We will disregard "loopers" which perform multiple loops in the detector before depositing all their energy, as we will end up looking at the highest p_T particles in an event, so we only worry about particles which eventually leave the inner detector, which means $|\frac{T}{2D}| < \frac{\pi}{2}$, as the particles are on the initial arc of their circular path when they leave the detector.

For twists, $\phi \rightarrow \phi - sz$, so

$$\phi' = \phi - sz = \frac{t}{2D} - sv_z t = t \left(\frac{1}{2D} - sv_z \right) = \epsilon t. \quad (\text{A.12})$$

Using this we can easily get how the x and y components of the particle's position evolve in time in the frame with a twist by returning to Cartesian coordinates and using equation A.7 to replace r. We derive that

$$x = \sqrt{2} D v_T \cos(t\epsilon) \sqrt{1 - \cos \frac{t}{D}} \quad (\text{A.13})$$

$$y = \sqrt{2} D v_T \sin(t\epsilon) \sqrt{1 - \cos \frac{t}{D}}. \quad (\text{A.14})$$

We take the formula for the curvature of a curve parameterized in Cartesian space,

$$\kappa = 1/r_c = \frac{|x'y'' - y'x''|}{\sqrt{x'^2 + y'^2}^3}, \quad (\text{A.15})$$

and we plug in our handy formulas for x and y with twists included. This results in

$$\kappa = 1/r_c = \left| \frac{\sqrt{2}\epsilon}{v_T} \frac{(-4\epsilon^2 D^2 + 1) \cos(\frac{t}{D}) + 4\epsilon^2 D^2 + 3}{((-4\epsilon^2 D^2 + 1) \cos(\frac{t}{D}) + 4\epsilon^2 D^2 + 1)^{\frac{3}{2}}} \right| \quad (\text{A.16})$$

At first glance, this looks like the curvature of the particle paths are not simply transformed back into circles with a different curvature. Digging deeper, one can check that for nonzero values of v_T , D , and ε , the denominator does not have any zeros. When we turn off the twists, we get $\varepsilon = \frac{1}{2D}$, and in that case,

$$\kappa \left[\varepsilon = \frac{1}{2D} \right] = \left| \frac{1}{Dv_T} \right| = \left| \frac{qB}{p_T} \right| \quad (\text{A.17})$$

which is both constant for all time and indeed captures the intuition that the higher p_T particles will have a lower curvature, but with a higher magnetic field, the particles would curve more. What about the opposite limit? As $|s| \rightarrow \infty$, we get

$$\kappa[|s| \rightarrow \infty] = \left| \frac{qB}{\sqrt{2}p_T \sqrt{1 - \cos \frac{t}{D}}} \right| = \frac{1}{r(t)} \quad (\text{A.18})$$

where the final equality comes from equation A.7. We see that in the completely unphysical case that the detector is infinitely twisted, we see that every point the particle would trace is warped into a concentric circle with the radii of its distance from the beam axis. In reality we only sample the particle's path at the discrete inner detector radii, but this is not a case we will be considering for the physical detector; it was just to verify the curvature formula makes sense.

So why does it appear that the radius of curvature of the particle's path with the twist appears to change with time? To answer this, we recast equation A.16 in the following form with the help of equation A.7:

$$\kappa = 1/r_c = \left| \frac{\sqrt{2}\varepsilon}{v_T} \frac{4 + (4\varepsilon^2 D^2 - 1) \frac{r(t)^2}{2D^2 v_T^2}}{\left(2 + (4\varepsilon^2 D^2 - 1) \left(\frac{r(t)^2}{2D^2 v_T^2}\right)\right)^{\frac{3}{2}}} \right|. \quad (\text{A.19})$$

Let us check the size of the term $(4\varepsilon^2 D^2 - 1) \frac{r(t)^2}{2D^2 v_T^2}$, found in the numerator and denominator. We will be looking at the highest momentum particles in a collision, but to be conservative, let us assume that p_T is no less than 1 GeV/c. Let us also assume that s is smaller than 0.003/meter, as this already means approximately 3mm of curvature along the edge of the inner detector. The maximum pseudorapidity of the inner detector is 2.5, so we use that for η . Lastly, the outer shell of the inner detector has a radius of approximately half a meter, so we use this for $r(t)$, and a magnetic field of 2 Tesla runs through the detector. Once we plug in all of the numbers, this term is approximately $1.65(10)^{-4} + 5.44(10)^{-3} * \frac{\text{GeV}/c}{p_T}$. Thus, based on our assumption that any relevant p_T is above 1 GeV/c, we see that this term is $O((10)^{-3})$.

Thus, as we have seen, we can disregard the term proportional to $r(t)$ in both the numerator and denominator with very small corrections on the final curvature. The result is that for particles with high enough p_T ,

$$\kappa = 1/r_c = \frac{2\varepsilon}{v_T} = \frac{1}{Dv_T} - 2s * \sinh \eta = \kappa_0 - 2s * \sinh \eta. \quad (\text{A.20})$$

Now that we have the final curvature that would be recorded from the twist, what effect does this have on measurements? The curvature of the track corresponds directly to the p_T of the track from equation A.17, so equation A.20 can be rewritten as a relationship between the twisted transverse momentum p'_T and the "ideal" transverse momentum p_T^0 as

$$\left| \frac{qB}{p'_T} \right| = \left| \frac{qB}{p_T^0} - 2s * \sinh \eta \right| \quad (\text{A.21})$$

or, more usefully, as

$$p'_T = p_T^0 \left| 1 - \frac{2sp_T^0}{qB} \sinh \eta \right|^{-1} = p_T^0 |1 - 2sv_z^0 D|^{-1} = p_T^0 |2D\varepsilon|^{-1}. \quad (\text{A.22})$$

